2nd Revision

XRD-TEM-AEM comparative study of n-alkylammonium smectites and interstratified minerals in shallow-diagenetic carbonate sediments of the Basque-Cantabrian Basin

FERNANDO NIETO[1], XABIER ARROYO[2] AND JAVIER AROSTEGUI[3]

[1] Departamento de Mineralogía y Petrología, IACT, Universidad de Granada-CSIC, Av. Fuentenueva s/n, 18002, Granada, Spain. nieto@ugr.es

[2] CAI de Técnicas Geológicas, Universidad Complutense de Madrid, C/ José Antonio Novais no. 2, 28040, Madrid Spain.

[3] Departamento de Mineralogía y Petrología, Facultad de Ciencia y Tecnología, Universidad del País Vasco/EHU, Apdo. 644, 48080, Spain.

Abstract

The validity of the application of the *n*-alkylammonium method to carbonate-rich lithologies was checked by means of a double comparison: First, the method was applied to samples studied by XRD and HRTEM. Second, these results were compared with the chemical compositions obtained independently by analytical electron microscopy (AEM) from single grains of smectites and I/S. Marl and marly limestone samples corresponding to the R0 and R1 illite/smectite mixed-layer (I/S) stages of diagenetic evolution have been analyzed by the *n*-alkylammonium method. Forty samples were taken and analyzed by routine X-ray diffraction (XRD) methods. The complete series from n_c:6 to n_c:18 has been used for XRD determination on eight samples, yielding layer charges of 0.32 to 0.39 afu for

the expandable component (formula based on $O_{10}(OH)_2$). Lattice-fringe images have been obtained under TEM from four selected samples treated with n_c:8 and n_c:14 alkylammonium, which are the best chain lengths for discrimination, according to the XRD results. The same type of interlayer configuration (mono-, bi- or pseudotri-layer) has been found by XRD and TEM in all cases. A comparison of the alkylammonium method layer charges with those calculated from formulas determined by AEM on single clay particles has revealed a good general agreement between the two independent methods; however, results from the alkylammonium method are 3 to 14% lower than those from AEM. This disparity is qualitatively in agreement with the literature, but the difference is clearly lower, presumably due to the use of specific *in-situ* analyses (which are contamination-free) instead of whole analyses of separates. The good agreement among the three methods validates their use for carbonate-rich lithologies. Layer charge increases with depth through the R0 stadium, but stabilizes, with no further increase, when the R1 stadium is reached; this change in behavior may be related with qualitative differences in the transformation mechanism.

Keywords: Illite-smectite mixed-layer, diagenesis, layer charge, marl, limestone

Introduction

Layer charge is a significant parameter in smectites and related minerals. It plays a fundamental role in edaphic environments as it determines the exchange capacity between the mineral component and fluids of soils. The diagenetic environment is characterized by the evolution from smectite (a low-charge 2:1 phyllosilicate) to high-charge micas. Therefore, the layer-charge evolution of smectite and illite-smectite mixed-layers (I/S)

during diagenesis is an interesting topic for which exact determination methods are necessary.

Nevertheless, a direct chemical determination is not simple due to the heterogeneous nature of clays and the very small grain size of smectites. The alkylammonium ion exchange method (Lagaly 1994; Mermut and Lagaly 2001) is a powerful tool that can be applied as a pre-treatment to X-ray diffraction (XRD) and/or high-resolution transmission electron microscopy (HRTEM) samples. Alkylammonium ions are able to enter into the interlayer space of 2:1 phyllosilicates, replacing the interlayer cations (Mermut and Lagaly 2001). They can adopt different configurations depending on the layer charge and the length of the alkylammonium chain, which may be prepared with 6 to 18 carbon atoms. The different configurations can be recognized in XRD and HRTEM studies by their characteristic d_{001} basal spacing. Therefore, the transition from one configuration to another occurs for different lengths of the alkylammonium chain, depending on the layer charge. A complete determination would require sample treatment with all the *n*-alkylammonium (hereafter, n_c: refers to the number of C atoms in the alkylammonium chain); the identification of n_c: for which the transitions occur would allow a determination of the layer charge. Due to heterogeneities in the layer charge at the sample level, the transition can occur in the range between two non-consecutive n_c:alkylammoniums.

The method has been applied to the expandable component of illite-smectite mixed-layers (I/S) (Lagaly 1979; Cetin and Huff 1995; Inoue et al. 2005). In such cases, a good knowledge of the proportion of S layers in the I/S is necessary to calculate the resulting d_{001} for the different alkylammonium configurations.

In HRTEM images, layer spacing can be directly measured. Smectites or I/S treated with alkylammonium are able to maintain, at least partially, their expanded spacing, characteristic

of each configuration under the microscope vacuum. Therefore, the method can also be applied to HRTEM samples (e.g. Rühlicke and Niederbudde 1985; Bell 1986; Vali et al. 1994; Murakami et al. 2005, Schumann et al. 2014). Sears et al. (1998) and Shata et al. (2003) combined XRD and HRTEM to determine the layer charge of I/S in lutitic samples, showing the complementary character of the two techniques. The study by Shata et al. (2003) identified minor smectite layers indiscernible by other methods in the transition from diagenesis to metamorphism.

Direct determination of the layer charge from the chemical composition of the sample would only be possible from monomineral samples. Even so, in the usual case of a non-homogeneous smectite composition in the sample, the average value would ignore the differences between the various grains or areas in a grain. Analytical electron microscopy (AEM) allows determination of the individual *in-situ* composition of any grain or specific area in the sample (e.g. Nieto et al. 1996; Drief and Nieto 2000). Therefore, the layer charge obtained by the alkylammonium ion exchange method can be compared with that obtained from the chemical composition determined by AEM on single clay particles.

Studies on the evolution of layer charge in diagenetic environments (with occasional comparisons between the various techniques) have been carried out chiefly on bentonite and shale lithologies, with studies on carbonate lithologies, such as marls, remaining very scarce in spite of the diagenetic retardation generally invoked for these cases (Ferreiro Mählmann et al. 2012, Arostegui et al. 2006).

To our knowledge, the applicability of the layer-charge determination by the alkylammonium ion exchange method to marls and/or carbonate lithologies has never been checked in spite of their abundance in diagenetic sequences and their purported diagenetic retardation. In addition, the employment of AEM to obtain contamination-free chemical

compositions of individual grains and to determine the degree of heterogeneity at the sample level is lacking in all the comparative studies performed until now. Therefore, the doubt remains about the critical role of possible contamination by other phases and internal chemical heterogeneities in the differences between layer charges determined by chemical analyses and those determined by the alkylammonium ion exchange method.

The Basque-Cantabrian Basin (northern Spain) is a suitable site to study diagenetic evolution in marls (Arostegui et al. 1991, 2006). It is a continuous Cretaceous and Tertiary carbonate and fine-grained sequence showing a complete evolution from the pure smectite stadium to R3 I/S, well exposed both in surface outcrops and in oil exploration boreholes.

The aim of this paper is to test the applicability of the alkylammonium ion exchange method for layer-charge determination in marls and marly-limestones of the Basque-Cantabrian Basin by means of a double comparison. First, the method is applied to samples studied by XRD, using the complete set of n_c:-alkylammonium, then comparing these results with those obtained in HRTEM for selected values of n_c:. Second, these results are compared with those obtained independently from the chemical compositions of smectites and I/S by AEM. Finally, the results provide information about diagenetic evolution in carbonate lithologies.

Materials and methods

Samples

Two sections (CS and KG) separated by approximately 10 km (representing the Upper Cretaceous materials of the Basque-Cantabrian Basin in the province of Alava) were selected for sampling based on previous geological and mineralogical studies (Sangüesa

1998, Sangüesa et al. 2000, and Arostegui et al. 2006). Samples free of superficial weathering were gathered from surface outcrops along the two sections (18 from CS and 22 from KG) according to their apparent clay contents; in most cases samples were marls, but when absent in the stratigraphic sequence, marly limestones were collected. After a preliminary routine clay analysis (see below), four samples from each of the two sections were selected for study. They represent the R0 and R1 stages of I/S evolution in each sequence; in the CS section, two samples correspond to the R0 stadium and two to the R1 stadium, and in the KG, three are R0 and one is R1.

X-ray diffraction

Sample preparation. Samples were washed with de-ionized water, air dried at room temperature, and gently crushed with a laboratory jaw-crusher. Randomly oriented powders of the bulk sample were used for characterization of whole-rock mineralogy. A solution of 0.2 *M* HCl was added to a suspension of crushed rock and continuously agitated for 20 minutes to eliminate carbonates. The <2 μm and <0.5 μm fractions were separated by centrifugation and then smeared onto glass slides. Samples were also saturated with K, Li, and Mg for specific determinations, using 1 *M* KCl or LiCl, or 0.1 *M* MgCl and washed free of cation salts. After Li treatment, samples were smeared on opaque fused silica slides, heated to 300ºC, and glycolated for 24 hours for the Greene-Kelly test. Glass capillaries were filled with 100 mg of the <2 μm fraction and 20% ZnO as internal standard for the b parameter determination.

XRD analysis. Clay minerals were identified according to the position of the (00l) series of basal reflections on XRD patterns of air-dried, ethylene-glycolated (EGC), dimethyl-sulfoxide treated, and heated (at 550°C for 1.5 hours) specimens (Moore and Reynolds

1997). XRD was performed using CuKα radiation with a Philips PW1710 diffractometer. The step size was 0.02º2θ with a counting time of 0.5 s per step. A Guinier-Huber camera was used to measure the (060) peak for the b parameter determination. The degree of order and smectite percentage of the I/S mixed layers were determined according to Moore and Reynolds (1997) based on the position and angular difference among the three first-order smectite peaks and the R1 super order.

Alkylammonium ion exchange treatment

Preparation of samples for XRD analysis. The complete series of *n*-alkylammonium chlorides (nc= 6-18, not commercially available, with the exception of 12 and 18) was prepared using a 1:1 mixture of the corresponding amine and ethanol and bubbling HCl to reach the equivalence point (Ruehlicke and Kohler 1981). Salt solutions were added to the <2 μm and <0.5 μm fractions after separation and Na-saturation to produce a 7–8 mg/ml suspension, which was vigorously shaken and kept at 65ºC for 24 hours. The process was repeated once and the samples washed with ethanol several times.

Preparation of samples for HRTEM study. After being separated and twice dehydrated with ethanol for 2.5 hours, the <2 μm fractions were embedded in Epon resin for the preparation of ultrathin sections following the method of Vali and Köster (1986). Ultrathin sections (700–900 Å) were prepared with an ultramicrotome using a diatome diamond knife. Two or three sections were selected and transferred onto Au TEM grids. The grids were transferred to 1.5 mL microtest tubes containing 1.0 mL of the n_c:8 and n_c:l4 alkylammonium-cation solutions diluted to 40% of the concentration prepared for XRD (Vali and Hesse 1990). The alkylammonium intercalation after embedding was preferred in order to avoid the problems described by Malla et al. (1993) and Schumann et al. (2014).

The closed tubes were stored in an oven at 65ºC and intermittently shaken for 20 minutes. Afterward, the grids (held with tweezers) were dipped 10–12 times into a beaker with distilled H_2O at 65ºC. The excess salt and H_2O on the grids were removed with filter paper.

Transmission electron microscopy

Lattice-fringe images of alkylammonium-treated samples. After the alkylammonium ion exchange treatment, the grids were carbon coated. TEM observations were obtained with a Philips CM20 equipped with an EDAX solid state EDX detector operating at 200 kV, with a LaB6 filament (Scientific Instruments Centre, University of Granada). Lattice-fringe images were obtained at 350,000–660,000X magnification following the procedures suggested by Buseck (1992). The mineral nature of each area was qualitatively identified by EDX analysis and selected area electron diffraction (SAED). Determination of d_{001} was carried out directly from the images with an estimated error of around 1Å.

Analytical electron microscopy (AEM). Quantitative analyses were obtained from powdered portions prepared using C-coated gold grids. In this kind of preparation, thin individual grains of minerals are scattered onto the grid with the (001) layers parallel to the sample surface. The microscope was operated in TEM mode for the identification and selection of different grains. Scanning TEM mode was used for quantitative analyses of particles with a 5 nm diameter beam and a 1x1 μm scanning area. Smectite and I/S grains were identified by their chemical composition. Two different counting times (30 s and 200 s) were used to minimize alkali-loss problems because short counting times improve reproducibility for K and Na (Nieto et al. 1996). Albite, biotite, spessartine, muscovite, olivine, and titanite standards were used to obtain K-factors for the transformation of intensity ratios to concentration following the procedures of Cliff and Lorimer (1975).

Results

Basic clay mineralogy

The results acquired on new surface samples coincide with those previously obtained on borehole samples (Sangüesa 1998; Arostegui et al. 2006), with the sole difference of additional detail due to improved methodology; the reader is referred to these previous publications for a more detailed description.

The whole-rock mineral composition is dominated by carbonates, chiefly calcite, with a minor (but appreciable) presence of dolomite in some samples from the CS section. Quartz and phyllosilicates are also abundant in all the samples. Albitic plagioclase is present along the two sections and K-feldspar in the upper part of the stratigraphic columns.

The clay mineralogy is dominated by micas, smectite, and I/S, with minor chlorite and kaolinite, more abundant at the sequence bottoms. Chlorite/smectite mixed layers (C/S) also occur in the lower part of the CS section. Figure 1 shows the evolution of the order and smectite-layer percentage of I/S along the two sections. At the bottom of the two sections, discrete smectite or R0 I/S are absent. Hereafter, these parts of the stratigraphic columns are considered as the R1 stage. Nevertheless, after a detailed decomposition of the XRD diagrams, minor quantities of R1 I/S have also been identified in the samples corresponding to the R0 stage. The coexistence at the sample level of more than one type of I/S is not new and has in fact been documented in the I/S literature in numerous papers (Bethke and Altaner 1986; Bethke et al. 1986; Brusewitz 1986; Nieto et al. 1996; Sato et al. 1996; McCarty et al. 2009; Ferrage et al. 2011; Do Campo et al. 2014). The evolution of the smectite-layer percentage in I/S shows the classic pattern of diagenetic environments

(Hower et al. 1976), with no variation in the shallower part and values of around 90% S, a second part showing a steady increase in illite layers, and the disappearance of smectite R0 in the R1 stage.

Treatment with glycerin, after homoionization with Mg, has produced similar results to treatment with EGC, which rules out the presence of vermiculite layers (Moore and Reynolds 1997). After homoionization with K, samples treated with EGC expand to more than 15 Å, classifying the smectites as low charge *sensu* Christidis and Eberl (2003). The Hofmann-Klemen treatment with Li (Greene-Kelly 1952) basically preserved the swelling nature of smectites; therefore, they are more beidellitic than montmorillonitic. The study of the (060) region, using decomposition methods, has shown a b parameter for smectites of circa 9 Å, with an absence of corresponding peaks in the 9.15 Å region; consequently, a dioctahedral character may be deduced for smectites and I/S. No significant difference was found for the treatments described in this paragraph between the results obtained for the <2 and <0.5 μm fractions.

Alkylammonium ion exchange XRD analysis

Selected samples from the basic clay mineralogy study have been treated with the entire set of *n*- alkylammonium for the <2 μm and <0.5 μm fractions. The same treatment was repeated for the two fractions on samples prepared according to the Hofmann-Klemen treatment (Greene-Kelly 1952). Figure 2 shows the XRD diagrams of the <2 μm fraction of a representative sample of the R0 stage, intercalated with the complete series of *n*-alkylammonium. Numerous coexisting mineral phases produce overlapping XRD peaks in the samples, making it necessary to interpret the diagrams with the aid of decomposition procedures (Fig. 3 and 4). After this procedure, the d_{001} spacing of smectites for the different

239 n_c: values of alkylammonium can be identified, and therefore the values of n_c: at which the
240 transition from monolayer to bilayer configurations occur can be determined (Fig. 5).

241 For samples corresponding to the R0 stage, two smectites can be recognized with
242 different d_{001} spacing in the n_c: zone in which the transition occurs (Fig. 2 and 3). For the
243 case of sample 1CS6 (shown in the figures), the specimen treated with alkylammonium n_c:8
244 shows only one smectite peak at 13.56 Å, which is broken up into two peaks for n_c:9 and
245 n_c:10 at 13.60 Å and 17.69 Å respectively. The specimen treated with n_c:11 again shows
246 only one peak at 17.70 Å, corresponding to the left one of those present in n_c:9 and n_c:10.
247 This behavior is interpreted in Figure 5 in terms of Sm1 and Sm2. Consequently, the two
248 smectites show a different value for the layer charge. Gier et al. (1998) also found two
249 smectites with different layer charges coexisting in the same samples from the Molasse
250 Basin in Austria.

251 Some of the spacing in the n_c: transition zone shows intermediate values between those
252 corresponding to the two configurations (e.g. Sm1 for samples 1CS6 and 2KG6, see Fig. 5).
253 As previously interpreted in the literature and confirmed by our TEM images (see below),
254 this is the result of a charge heterogeneity of smectite layers at the sample level.

255 Table 1 presents the layer-charge values for the <2 μm and <0.5 μm fractions in samples
256 before and after the Hofmann-Klemen treatment (Greene-Kelly 1952), calculated following
257 the procedure by Lagaly (1994). The XCharge software (Hofmann et al. 2002) has been
258 used to calculate layer charge from the n_c: values at which the transition from monolayer to
259 bilayer configurations occurs. Two different values have been calculated for those cases in
260 which two peaks have been found in the transition zone, completing their change at different
261 n_c: values.

Low-charge values, in the range of 0.32 to 0.39 atoms per formula unit (afu), expressed on the basis of 11 oxygens, were found for major smectite (Sm1) and of 0.37 to 0.41 for minor smectite (Sm2). After the Li treatment (Greene-Kelly test), these values decrease slightly to 0.27–0.32 for Sm1 and to 0.34–0.41 for Sm2, indicating most of the charge is present in the tetrahedral layer, confirming the beidellitic nature of the expandable components. The results for the <0.5 μm fraction are equal or very similar to those of the <2 μm fraction (stated above).

The right part of Figure 2 shows the XRD diagrams of the <2 μm fraction of a representative sample of the R1 stage, intercalated with the complete series of *n*-alkylammonium. For the interpretation and calculation of sample layer charge corresponding to the R1 stage, we followed the same procedure described above for the R0 stage. Figure 4 shows the decomposition procedure for sample 3CS3. The interpretation of the spacing at which transition occurs is based on this procedure. Figure 5 presents the corresponding d_{001} spacing for the different n_c: of alkylammonium for samples 3CS3 and 3CS6, representative of the R1 stage. The expected d_{001} values for the two kinds of configurations were calculated according to the proportion of S layers in the I/S mixed layers (see Fig. 1). For example, the monolayer configuration of the alkylammonium ions in sample 3CS3 (35% S in I/S mixed-layer) would correspond to an average d-spacing of 11.26 Å (13.6 Å·35% S + 10 Å·65% I).

Low-charge values (in the range of 0.33 to 0.38 afu) were obtained on the <2 μm fraction for the R1 stage samples (Table 1), with no significant differences in relation to the <0.5 μm fraction. The Li treatment (Greene-Kelly test) only slightly reduces these values; therefore, the expansive component of the R1 I/S is also confirmed to be predominantly beidellitic.

Long-chain *n*-alkylammoniums can expand degraded or low-charge illite (Laird et al. 1987; Vali and Köster 1986). According to these authors, the expanded layers are true illitic

layers and the swelling mechanism is different from that of smectitic layers, leading to the so-called paraffin-type configuration. Our samples also show peaks corresponding to this expanded phase for n_c: ≥ 10 (Fig. 2), with spacings related to the chain length and the illite interlayer charge (Ghabru et al. 1989; Mermut 1994). Two different swelling illites, with diverse layer charges and paraffin-type configuration of the alkylammonium ions, have been recognized.

Lattice-fringe images of alkylammonium-treated samples

Samples 1CS6 and 2KG6 have been selected as representative of the R0 stadium for the HRTEM study. 3CS3 and 3CS6 were chosen for the R1 stadium. For each of the samples, one specimen treated with a short-chain alkylammonium (n_c:8) and a second one treated with a long-chain one (n_c:14) have been studied. The main aim was to measure a great number of interlayer spacings to corroborate and complete the XRD study. Figure 6 shows the typical low-magnification texture of the samples, cut with the diamond knife and treated with the corresponding *n*-alkylammonium. The original sample texture is lost during this preparation procedure. A great number of phyllosilicate packets, separated by voids produced by the knife, are shown in the images, allowing numerous layer spacings to be measured. The following description is based on the study of hundreds of lattice images, from which some representative ones are presented.

In addition to smectites and I/S, all the rest of the clay mineral phases described in the XRD section have been recognized in the TEM images, including expandable illites, C/S mixed-layers, and non-expandable phases, such as micas and chlorite. As they are beyond the scope of this paper, they are not described.

Since R (-order nomenclature was defined for XRD, it has a statistical meaning. Therefore, it is inadequate to describe short-range order, as identified in lattice-fringe images. Consequently, we have adopted the nomenclature proposed by Bauluz et al. (2000), in which In means that n illite layers are separated by smectite layers.

Sample 1CS6 (R0 stadium). Most of the lattice fringes of the specimen treated with n_c:8 alkylammonium show spacings between 12 and 14 Å (Fig. 7), characteristic of a monolayer configuration (13.6 Å). Spacing lower than the theoretical one can be found as a result of a partial deterioration of alkylammonium chains due to electron beam damage (Vali and Hess 1990). Smectite packets are formed by 2–10 curved layers, showing their characteristic highly defective nature. Some minor cases (<5%) of packets with spacings greater than 14 Å may be interpreted as a bilayer configuration produced by heterogeneity in the smectite charge.

Most of the lattice fringes in the specimen treated with n_c:14 alkylammonium show spacings between 17 Å and 22 Å, characteristic of the transition from bilayer (17.7 Å) to pseudo-trilayer configurations (22.7 Å).

In both the specimens treated with the short and long chains, lateral or transverse spacing changes are a consequence of various alkylammonium-layer configurations, consistent with local differences in smectite charge, the result of compositional differences between the smectite layers. This heterogeneity was predicted by the XRD analysis as intermediate spacing between the spacings characteristic of the two different configurations.

In addition to these smectite-type packets, I1 I/S have also been recognized both in the short- and long-chain alkylammonium-treated samples. In the short-chain specimens, the predominant spacing is 24 Å (10 Å from illite + 14 Å from monolayer smectite), with minor

27 Å (10+17). In the long-chain specimens, spacings are between 27 Å and 32 Å (10 Å from illite + 22 Å from pseudo-trilayer smectite).

Sample 2KG6 (R0 stadium). The lattice fringes of the specimen treated with n_c:8 alkylammonium show spacings of 13–18 Å (Fig. 8), characteristic of the transition from monolayer (13.6 Å) to bilayer (17.7 Å) configurations, partly affected by electron beam damage. Similarly to the afore-described sample, smectite packets are formed by up to 10 curved layers, showing a highly defective nature. Packets of only 2–5 layers are the most common. Lateral transitions have been observed between the two extreme spacings, corresponding to the two configurations.

The specimen treated with n_c:14 alkylammonium shows spacings of 17 Å to 22 Å (Fig. 9), characteristic of the transition from bilayer (17.7 Å) to pseudo-trilayer configurations (22.7 Å). In Figure 9, an example of lateral transition from 22 Å (pseudo-trilayer) to 18 Å (bilayer) can be noted, which implies a layer charge lateral change.

In both the short- and long-chain alkylammonium-treated samples, I1 I/S have been recognized. A specimen treated with n_c:8 has a spacing of 27 Å (lower part of Fig. 8), which corresponds to the sum 10+17 Å. A specimen treated with n_c:14 has a spacing of 28 Å (lower part of Fig. 9) or 32 Å, which corresponds to the sum of one illite unit and one smectite unit showing respectively a bilayer or pseudo-trilayer configuration.

Most of the I/S have a regular I1 arrangement with a 1:1 proportion of illite/smectite units, but minor disordering may be present, such as an extra smectitic layer in the lower part of the afore-mentioned I/S in Figure 9. Both in this sample and in the afore-described 1CS6, illite units of the I/S mixed-layer do not have any swelling effect after the alkylammonium treatment.

Samples 3CS3 and 3CS6 (R1 stadium). The two samples of this stadium show similar characteristics and are therefore described together.

The specimens treated with n_c:8 alkylammonium show packets of regular I1, I2, or I3 I/S, constituted by 2–8 structural units. In some of the packets, a 1:1 ratio between illite and smectite layers is observed; however, excess illite layers are very common (Fig. 10). The layers of the two components can often be distinguished not only by the spacing, but also by the difference in contrast. Illite layers show 10 Å spacing. Smectite layers have a 14 Å monolayer configuration in most units of sample 3CS3 (Fig. 10) and both a 14 Å monolayer or 17 Å bilayer configuration for sample 3CS6.

Specimens treated with n_c:14 alkylammonium show packets with similar characteristics to those described for the short-chain alkylammonium, with the only difference being the d_{001} spacings of the smectite layers, which in these cases correspond to the bilayer to pseudo-trilayer transition with spacings between 18 and 21 Å (Fig. 11a and b). Illite layers are not expanded. I1 periodicity with a 1:1 illite/smectite ratio is not rare (Fig. 11b), but there is usually one smectite layer and more than one illite layer. Figure 11a shows I≥3 periodicities with one smectite layer and 3, 4, 5, or 6 illite layers. The smectite layer is commonly open due to beam damage. The extent of the I≥3 domains is greater than for the I1 ones, both normal and parallel to the layers.

Chemical composition of I/S determined by analytical electron microscopy (AEM)

According to XRD and HRTEM analyses, both smectite and R1 I/S are present in samples corresponding to the R0 stadium; therefore, it was necessary to establish a criterion to classify compositions obtained by AEM into one of the two groups. As samples corresponding to the R1 stadium are characterized by the absence of smectite or R0 I/S, we

have established the chemical characteristics of R1 I/S based on these samples and the identification of some grains by SAED: interlayer charge ≥ 0.5 atoms per formula unit (afu) and/or Si < 3.60±0.05 afu.

Smectite or R0 I/S mixed-layer. The chemical compositions for the five samples analysed, corresponding to the R0 stadium, are presented in Table 2. The composition is highly variable between different grains in the same sample and from sample to sample, that is, the smectite composition is highly heterogeneous. Although generally true, there are some common characteristics regardless of the sample: (1) Compositions are clearly dioctahedral, with most octahedral sums not too far from the theoretical value of 2 afu; (2) interlayer charge sums are low, ranging from 0.27 to 0.50 afu, with most of the values between 0.35 and 0.45 afu; (3) K is the majority interlayer cation, but Na and Ca are also present in significant amounts; (4) Si is lower than 4, ranging from 3.47 to 3.90 afu, that is, significant Al^{IV} substitution is present; (5) Fe and Mg are low — the latter in particular is normally lower than Al^{IV}. The two last characteristics indicate most of the analyses are beidellitic.

R1 I/S mixed-layer. The chemical compositions for the eight samples analysed, corresponding to the R0 and R1 stadium, are presented in Table 3. Similarly to smectites, the compositions are highly heterogeneous. In relation to smectites or R0 I/S, the R1 compositions show, as expected, lower Si and higher Al contents, together with higher interlayer charges. The compositions are clearly dioctahedral. K is the dominant interlayer cation, but Na and Ca are also present. R1 IS has higher K and Na in comparison to R0 IS, but Ca is similar in R1 and R0 and lower than K and Na. Fe and Mg contents are low and similar to those found for smectites.

Discussion

Alkylammonium ion exchange: XRD *vs* HRTEM analyses

Although XRD and lattice-fringe images obtained by TEM provide information about the same physical parameter (that is, the d_{001} spacing), one must bear in mind the significantly different nature of the two kinds of specimens used for each of the methods. The measurements by XRD are highly representative; they are the result of an average value of millions of crystals in the specimen. Lattice-fringe images correspond to individual crystals and each of the images can be related to the physical nature of the crystal measured. Therefore, the two methods are complementary, the latter recognizing the physical entity being measured and the former extending the measured values to a huge number of crystals, adding the representativeness the other method lacks.

Below, the coherence of the two types of measurements is analyzed and facts that can be deduced from only one of the techniques are considered to illustrate their complementary nature.

Figure 12 compares the interlayer arrangement obtained by each of the two methods. The selection of one short and one long alkylammonium has provided examples of the three kinds of arrangements. Complete correspondence can be noted, with the same kind of arrangement obtained in all cases by the two methods for the two lengths of chain.

The selection of samples and chain lengths also included cases that, according to XRD, corresponded to transitions between two kinds of configurations in order to determine the physical nature of this transitional pattern from direct images of the crystals. Figures 8, 9, and 11a show the coexistence of the spacing for two kinds of configurations in an area of a few hundred angstroms, in some cases in the same packet, which have a lateral transition

427 from one kind of arrangement to the other. In these cases, which correspond to I/S types R0
428 and R1, XRD identified intermediate spacing between the spacings of the two kinds of
429 configurations. Therefore, the lattice-fringe images of individual crystals corroborate that
430 intermediate spacing in XRD is the result of a weighted average between two extreme
431 arrangements: monolayer and bilayer. In cases in which the smectite layer charge has a
432 range that covers the values corresponding to two different arrangements, each of the
433 individual layers adopts one or the other depending on its exact layer charge (Schumann et
434 al. 2014). As shown in Figures 8 and 9, such differences in composition may even affect the
435 same layer in two different locations.

436 As presented in the XRD results, two different smectites (termed Sm1 and Sm2, Fig. 5)
437 were identified and interpreted as corresponding to two different layer-charge values.
438 Lattice-fringe images have not differentiated them using microscopic methods. For sample
439 1CS6, the kind of configuration predicted by XRD for the two smectites was the same for
440 both the n_c:8 and n_c:14 (Fig. 5), and therefore no difference was expected between them in
441 the lattice-fringe images; for sample 2KG6, the transition between the monolayer and
442 bilayer was identified for Sm1 and the bilayer configuration for Sm2 (Fig. 5), and therefore
443 the crystals showing a bilayer configuration in HRTEM may correspond either to Sm2 or to
444 the higher charge fraction of Sm1, with no other additional possible criteria to differentiate
445 them.

446 In the treatment of XRD data corresponding to R1 I/S, it was necessary to assume, as a
447 starting hypothesis, that illite layers were not affected by the alkylammonium treatment and
448 maintained their 10 Å spacing. Consequently, the theoretical spacing for any kind of
449 interlayer arrangement was calculated according to the ratio of smectite and illite layers,
450 considering 10 Å for illite and the corresponding spacing for each kind of expanded

smectite. In Figures 8, 9, 10, and 11 we show R1 or R3 I/S in which the lattice spacing matches the sum of a given number of 10 Å layers (the illite part of the interlayers) and one smectite layer with the spacing corresponding to its alkylammonium interlayer configuration. Therefore, the assumption of no swelling of the illite layers has been demonstrated to be correct, and the suggested means for calculating the theoretical spacing of each kind of configuration is apparently correct as well.

The existence of R1 I/S coexisting with R0 I/S in the samples corresponding to the R0 stadium was deduced during the XRD study, but it was impossible to know at which n_c: of alkylammonium the transition occurred and therefore to calculate their layer charge. Lattice-fringe images have corroborated the presence of both types in the samples (Fig. 8 and 9) and even confirmed that the smectite layers have the same kind of configuration as in R0 I/S for the same sample and alkylammonium length (Fig. 12), with the only possible exception being sample 2KG6 for n_c:8 (this specimen shows only a bilayer configuration for R1 and a monolayer-bilayer transition for R0).

Other data impossible to obtain in the XRD study were the type of configuration with long chain alkylammonium of R1 in the two samples of the R1 stadium (Fig. 5) due to the overlapping expanded illite peaks (Fig. 2b). Lattice-fringe images identify a bilayer–pseudo-trilayer transition for the two specimens (see Fig. 13).

The case of R>3 I/S is also interesting. The alkylammonium treatment did not allow study of the layer charge by XRD due to their near coincidence in the diagrams with illite and/or detrital micas. Nevertheless, they have been identified in lattice-fringe images (Fig. 11a) showing a bilayer–pseudo-trilayer transition for the n_c:14 specimen. Therefore, this identification revealed that R>3 I/S has the same configuration as R1 in the same sample and presumably a similar layer charge for their respective smectite components.

In conclusion, the comparative study of XRD and lattice-fringe images has shown complete coincidence in the type of interlayer configuration of alkylammonium determined by the two methods. They are also complementary, particularly regarding phases in minor proportions or affected by overlap in the XRD diagrams of peaks corresponding to other minerals.

Layer charge determined by alkylammonium treatment *vs.* the structural formula determined by analytical electron microscopy

Layer charge determined by alkylammonium treatment has frequently been compared with other methods such as cation exchange capacity, specific surface area, and structural formula, of which only the structural formula is completely independent. Nevertheless, this method needs chemical analyses of pure fractions, until now performed by different spectroscopic methods such as ICP ((Laird et al. 1989; Cetin and Huff 1995) and XRF (Kaufhold et al. 2011). In all these methods, even slight contamination by crystalline or amorphous materials may be a source of error in the calculation of the formula.

Laird (1994) found that layer charge calculated from the structural formula is up to 40% higher than that calculated by the alkylammonium method. Kaufhold (2006), in agreement with previous findings by Köster (1977), considered that the results obtained from the formula are too high, while the alkylammonium method is able to offer more accurate results. Czímerová et al. (2006) did not find good agreement between the two kinds of values, attributing the differences to sample impurities and the various assumptions necessary to calculate layer charge from the chemical data.

After validating the equivalence of results obtained for the layer-charge values by the alkylammonium method in XRD and HRTEM, these results are compared with data

obtained by an external method, that is, the chemical composition determined using AEM. Figure 13 compares the results found in this study by the alkylammonium method (Table 1) with the layer charge calculated from the formulae obtained by AEM (Tables 2 and 3). As presented in the Results section, AEM shows a very heterogeneous chemistry for smectites and I/S, and therefore the values in Figure 13 are averages for each sample. In spite of this fact, good agreement can be observed in the figure.

In general, layer charge values calculated from the structural formula determined by AEM for smectites and R0 I/S are higher than with the alkylammonium method, but the two show similar trends. the alkylammonium method frequently yields lower values than those obtained directly from the structural formula (Laird 1994; Kaufhold 2006; Christidis, 2008), from around 20% lower (Lagaly 1981; Laird et al. 1989) to circa 25% (Cetin and Huff 1995; Wolters et al. 2009) and up to 40% (Laird 1994). In our case, the differences are lower, ranging between 3% and 14% (Fig. 13).

At least three different reasons could explain the lower values found with the alkylammonium method in the literature and in our study. (1) The alkylammonium method only measures the interlayer permanent charge, whereas chemical methods also quantify the variable charge in the broken borders and faces of the particles (Christidis, 2008); taking into account the very small grain size of smectite, one structural unit can represent more than 10% of the overall particle. (2) The minor illitic layers in the R0 I/S provide an additional charge, not taken into account by the alkylammonium method, which only measures the expandable component. (3) Given the heterogeneity of compositions at the sample level, the alkylammonium method measures the most abundant compositions; for example, the smectite 2 of samples 1CS6 and 2KG6 (Fig. 3 and 5) has not been taken into account in Figure 13, but it may contribute to the average value calculated from AEM data.

523 Recently, Kaufhold et al. (2011) analyzed by XRF various bentonites whose purity had
524 been checked by XRD. They found differences between the structural formula and the
525 alkylammonium methods of around 20%. They explained the differences between the two
526 methods as due to: (1) in the case of samples containing minor impurities, even in the <0.2
527 μm fraction, these contaminations can account for the larger deviations, but around 10%
528 difference still remains unexplained; (2) a variable charge, linked to the external surface of
529 the particles, is able to justify a significant part of this remaining difference; (3) the rest of
530 the divergence is explained by the existence of the so-called "non-exchangable, non-
531 structural cations".

532 In contrast to Kaufhold et al. (2011), we determined the chemical composition of the
533 smectites using AEM *in-situ* analyses of individual particles instead of whole analyses of
534 separated fractions. To our knowledge, this is the first comparison between the two methods
535 that directly uses the composition of individual particles and is therefore presumably free of
536 contamination. This is why our AEM results diverge from the alkylammonium values by
537 less than 10%, which is the value found by Kaufhold et al. (2011) when considering only
538 presumably contamination-free samples. According to Christidis (2008), this difference can
539 be explained by the variable charge in the borders and faces of the particles. The exact
540 meaning of the expression "non-exchangable, non-structural cations" is not completely
541 defined by Kaufhold et al. (2011), but could perfectly correspond to the cations linked to
542 non-expandable minor illitic layers in the R0 I/S.

543 In the case of I/S, the comparison is more complex as the alkylammonium method
544 determines exclusively the layer charge of the I/S expandable component, whereas the value
545 calculated from the formula includes the charge from both the illitic and smectitic
546 components. Therefore, to compare the two methods, we needed to subtract the layer charge

corresponding to the illite layers. To carry out these calculations, one must assume the percentage of illite layers (determined by the Moore and Reynolds 1997 method; Fig. 1) and a fixed layer charge for the illitic layers. Taking into account the IMA definition of illite (Rieder et al. 1998), we have considered 0.8 afu as a reasonable value, not far from those frequently cited in the literature (Srodon and Eberl 1984) for the illite charge. In spite of such approximate assumptions, the heterogeneity of I/S compositions and other numerous analytical problems, the values for the two samples of R1 I/S are comfortably similar for the two methods (Fig. 13). A slightly lower illite charge would be enough to justify the somewhat lower value obtained by AEM.

Another significant coincidence between the analyses by the two independent methods lies in the charge location between the tetrahedral and octahedral sheets. The comparison between the layer charge obtained by the alkylammonium method before and after the Greene-Kelly (1952) treatment revealed that the layer charge derives basically from the tetrahedral sheet (Table 1) as only small differences were found between them. The same conclusion can be drawn from the comparison between Al^{IV} and Mg values obtained by AEM (Tables 2 and 3).

Evolution of the layer charge in marls of the Basque-Cantabrian Basin

The joint application of the above-described methods has allowed the determination of the layer charge of the Upper Cretaceous marls and marly limestones of two sections of the Basque-Cantabrian Basin (Table 1, Fig. 13), together with their evolution with depth.

In the two sections, an upper part has been recognized containing major smectite or R0 I/S and minor R1 I/S and a lower part containing R1 I/S, in which smectite and R0 I/S are absent. Previous studies (Sangüesa 1998; Arostegui et al. 2006) had documented retardation

in the evolution of the smectite-illite system in relation to the depth and temperature reached by the materials due to their carbonate-rich nature. The layer charge determined in this study indicates that: (1) the layer charge is low for all the swelling materials (smectite and smectitic layers of I/S) in the two sections; (2) the upper parts of the two sections include a heterogeneous mixture of swelling phases whose layer charge increases progressively with depth; (3) the lower parts of the sections do not show an additional increase in charge with depth, with the layer charge determined being similar to that found at the bottom of the upper parts.

The described behavior indicates a change in the mechanism of transformation of smectitic to illitic layers coinciding with the final consumption of discrete smectite. Therefore, a qualitative change is implied when the R1 stadium is reached in the diagenetic evolution and the two stadia cannot be simply considered as two parts of a progressive process.

Application of the alkylammonium method to carbonate-rich lithologies. Implications

To our knowledge, the alkylammonium method has not yet been extended to marl or limestone rocks. As diagenetic processes in these types of rocks may be affected by significant retardation, it would be important to have an accurate method to determine layer charge in the abundant sequences in which this lithology is present. Therefore, one of the aims of this study has been to test the validity of the alkylammonium-based methods previously described in the literature for carbonate lithologies.

The data show coherent results, with d_{001} spacing wholly coinciding between XRD and lattice-fringe images when the same sample and the length of the alkylammonium chain are considered (Fig. 12). The comparison of these results with the *in-situ* compositions

595 determined by AEM has shown that the values measured by the alkylammonium method are
596 slightly lower than those calculated from the chemical formula. This conclusion is in
597 agreement with the literature although our difference is smaller than that previously
598 reported. This more similar behavior could be the consequence of the use of specific
599 analyses on individual particles, presumably less affected by contamination than
600 compositions obtained by more massive methods.

601 These results imply that the alkylammonium method can be applied to the smectite and
602 I/S in carbonate lithologies with the same kind of protocols, possibilities, and limitations as
603 those previously proposed for and applied to more pelitic lithologies. Moreover, it is
604 possible to successfully determine the layer charge of the expandable component in samples
605 with more than one type of coexisting mixed-layers (R0 and R1 I/S and/or C/S). In addition,
606 the good agreement among the results obtained by the three methods validate them and
607 confirm good accuracy and their possibility of application to a wide range of materials.

608

609 **Acknowledgments**

610

611 This work was financed by Research Projects CGL2011-30153-C02-01 and CGL2011-
612 23770 (Spanish Ministry of Science), and PAIDI-group RNM-179. The help of M.M. Abad-
613 Ortega (TEM/ AEM), Juan de Dios Bueno-Perez, and Concepción Hernandez-Castillo
614 (embedding of samples and ultramicrotome) of the Scientific Instruments Centre (CIC) of
615 Granada was fundamental for this study. We also thank Christine Laurin for revising the
616 English text.

617 **REFERENCES CITED**

618 Arostegui, J., Sanguesa, F.J., Nieto, F., and Uriarte, J.A. (2006) Thermal models and clay diagenesis
619 in the Tertiary-Cretaceous sediments of the Alava Block (Basque-Cantabrian basin, Spain).
620 Clay Minerals, 41, 791-809.
621 Aróstegui, J., Zuluaga, M.C., Velasco, F., Ortega-Huertas, M., and Nieto, F. (1991) Diagenesis of
622 the Central Basque-Cantabrian basin (Iberian Peninsula) based on illite-smectite
623 distribution. Clay Minerals, 26, 535-548.
624 Bauluz, B., Peacor, D.R., and Gonzalez Lopez, J.M. (2000) Transmission electron-microscopy
625 study of illitization in pelites from the Iberian Range, Spain - layer-by-layer replacement.
626 Clays and Clay Minerals, 48, 374-384.
627 Bell, T.E. (1986) Microstructure in mixed-layer illite/smectite and its relationship to the reaction of
628 smectite to illite. Clays and Clay Minerals, 34, 146-154.
629 Bethke, C.M., and Altaner, S.P. (1986) Layer-by-layer mechanism of smectite illitization and
630 application to a new rate law. Clays and Clay Minerals, 34, 136-145.
631 Bethke, C.M., Vergo, N., and Altaner, S.P. (1986) Pathways of smectite illitization. Clays and Clay
632 Minerals, 34, 125-135.
633 Brusewitz, A.M. (1986) Chemical and physical-properties of paleozoic potassium bentonites from
634 Kinnekulle, Sweden. Clays and Clay Minerals, 34, 442-454.
635 Buseck, P., Cowley, J., and Eyring, L. (1992) High Resolution Transmission electron microscopy
636 and associated techniques. Oxford Science Publications.
637 Cetin, K., and Huff, W.D. (1995) Layer charge of the expandable component of illite/smectite in K-
638 bentonite as determined by alkylammonium ion-exchange. Clays and Clay Minerals, 43,
639 150-158.
640 Christidis, G.E. and Eberl, D.D. (2003) Determination of layer-charge characteristics of smectites.
641 Clays and Clay Minerals, 51, 644-655.

642 Christidis, G.E. (2008) Validity of the structural formula method for layer charge determination of
643 smectites: A re-evaluation of published data. Applied Clay Science, 42, 1-7.
644 Cliff, G., and Lorimer, G.W. (1975) The quantitative analysis of thin specimens. Journal of
645 Microscopy, 103, 203-207.
646 Czimerova, A., Bujdak, J., and Dohrmann, R. (2006) Traditional and novel methods for estimating
647 the layer charge of smectites. Applied Clay Science, 34, 2-13.
648 Do Campo, M., Nieto, F., del Papa, C., and Hongn, F. (2014) Syn- and post-sedimentary controls on
649 clay mineral assemblages in a tectonically active basin, Andean Argentinean foreland.
650 Journal of South American Earth Sciences, 52, 43-56.
651 Drief, A., and Nieto, F. (2000) Chemical composition of smectites formed in clastic sediments.
652 Implications for the smectite-illite transformation. Clay Minerals, 35, 665-678.
653 Ferrage, E., Vidal, O., Mosser-Ruck, R., Cathelineau, M., and Cuadros, J. (2011) A reinvestigation
654 of smectite illitization in experimental hydrothermal conditions: Results from X-ray
655 diffraction and transmission electron microscopy. American Mineralogist, 96, 207-223.
656 Ferreiro-Mahlmann, R., Bozkaya, O., Potel, S., Le Bayon, R., Segvic, B., and Nieto, F. (2012) The
657 pioneer work of Bernard Kubler and Martin Frey in very low-grade metamorphic terranes:
658 Paleo-geothermal potential of variation in Kubler-Index/organic matter reflectance
659 correlations. A review. Swiss Journal of Geosciences, 105, 121-152.
660 Ghabru, S.K., Mermut, A.R., and Starnaud, R.J. (1989) Layer-charge and cation-exchange
661 characteristics of vermiculite (weathered biotite) isolated from a gray luvisol in northeastern
662 Saskatchewan. Clays and Clay Minerals, 37, 164-172.
663 Gier, S., Ottner, F., and Johns, W.D. (1998) Layer-charge heterogeneity in smectites of I-S phases
664 in pelitic sediments from the Molasse Basin, Austria. Clays and Clay Minerals, 46, 670-678.
665 Greene-Kelly, R. (1952) Irreversible dehydration in montmorillonite. Clay Minerals Bulletin, 1,

221-225.

Hofmann, H., Bauer, A., and Warr, L.N. (2002) XCharge: ein Programm zur Berechnung der Schichtladung und Schichtladungsverteilung niedrig geladener Phyllosilikate mit Hilfe der Alkylammonlum-Methode Grundlagen und Benutzerhandbuch (XCharge: A program for calculating layer charge and layer charge distribution of low-charged phyllosilicates using the alkylammonium method). Wissenschaftliche Berichte, FZKA 6744, 1-26.

Hower, J., Eslinger, E., Hower, M., and Perry, E. (1976) Mechanism of burial metamorphism of argillaceous sediments: 1. Mineralogical and chemical evidence. Geological Society of America Bulletin, 87, 725–737.

Inoue, A., Lanson, B., Marques-Fernandes, M., Sakharov, B.A., Murakami, T., Meunier, A., and Beaufort, D. (2005) Illite-smectite mixed-layer minerals in the hydrothermal alteration of volcanic rocks: I. One-dimensional XRD structure analysis and characterization of component layers. Clays and Clay Minerals, 53, 423-439.

Kaufhold, S. (2006) Comparison of methods for the determination of the layer charge density (LCD) of montmorillonites. Applied Clay Science, 34, 14-21.

Kaufhold, S., Dohrmann, R., Stucki, J.W., and Anastacio, A.S. (2011) Layer charge density of smectites - closing the gap between the structural formula method and the alkyl ammonium method. Clays and Clay Minerals, 59, 200-211.

Koster, H.M. (1977) Calculation of crystal chemical structural formulas of 2-1 layer silicates with particular consideration of measured interlayer charges and cation-exchange capacities - representation of charge-distribution in structure by means of triangular coordinates. Clay Minerals, 12, 45-54.

Lagaly, G. (1979) The "layer charge" of regular insterstratified 2:1 clay minerals. Clays and Clay Minerals, 27, 1-10.

690 -. (1981) Characterization of clays by organic-compounds. Clay Minerals, 16, 1-21.
691 -. (1994) Layer charge determination by alkylammonium ions. In A. Mermut, Ed. Layer Charge
692 Characteristics of Clays, 6, p. 1-46. The Clay Minerals Society, Boulder, Colorado.
693 Laird, D.A. (1994) Evaluation of structural formulae and alkylammonium method of determining
694 layer charge. In A. Mermut, Ed. Layer Charge Characteristics of Clays, 6, 79-104. The Clay
695 Minerals Society, Boulder, Colorado.
696 Laird, D.A., Scott, A.D., and Fenton, T.E. (1987) Interpretation of alkylammonium characterization
697 of soil clays. Soil Science Society of America Journal, 51, 1659-1663.
698 -. (1989) Evaluation of the alkylammonium method of determining layer charge. Clays and Clay
699 Minerals, 37, 41-46.
700 McCarty, D.K., Sakharov, B.A., and Drits, V.A. (2009) New insights into smectite illitization: A
701 zoned K-bentonite revisited. American Mineralogist, 94, 1653-1671.
702 Malla, P.B., Robert, M., Douglas, L.A., Tessier, D., and Komarneni, S. (1993) Charge heterogeneity
703 and nanostructure of 2:1 layer silicates by high-resolution transmission electron microscopy.
704 Clays and Clay Minerals, 41, 412-422.
705 Mermut, A.R. (1994) Problems associated with layer charge characterization of 2:1 phyllosilicates.
706 In A.R. Mermut, Ed. Layer Charge Characteristics of 2:1 Silicate Clay Minerals, 6, 105-127.
707 Clay Minerals Society Workshop Lectures, Boulder (Colorado).
708 Mermut, A.R., and Lagaly, G. (2001) Baseline studies of The Clay Minerals Society Source Clays:
709 Layer-charge determination and characteristics of those minerals containing 2:1 layers.
710 Clays and Clay Minerals, 49, 393-397.
711 Moore, D.M., and Reynolds, R.C.J. (1997) X-ray diffraction and the identification and analysis of
712 clay minerals. 378 pp. Oxford Univ. Press, New York.
713 Murakami, T., Inoue, A., Lanson, B., Meunier, A., and Beaufort, D. (2005) Illite-smectite mixed-

layer minerals in the hydrothermal alteration of volcanic rocks: II. One-dimensional HRTEM structure images and formation mechanisms. Clays and Clay Minerals, 53, 440-451.

Nieto, F., Ortega-Huertas, M., Peacor, D., and Arostegui, J. (1996) Evolution of illite/smectite from early diagenesis through incipient metamorphism in sediments of the Basque-Cantabrian Basin. Clays and Clay Minerals, 44, 304-323.

Rieder, M., Cavazzini, G., D'Yakonov, Y.S., Frank-Kamenetskii, V.A., Gottardi, G., Guggenheim, S., Koval, P.V., Muller, G., Neiva, A. M.R., Radoslovich, E.W., Robert, J.L., Sassi, F.P., Takeda, H., Weiss, Z., and Wones, D.R., 1998. Nomenclature of the micas. Canadian Mineralogist, 36, 1-8.

Ruhlicke, G., and Kohler, E.E. (1981) A simplified procedure for determining layer charge by the n-alkylammonium method. Clay Minerals, 16, 305-307.

Ruhlicke, G., and Niederbudde, E.A. (1985) Determination of layer-charge density of expandable 2-1 clay-minerals in soils and loess sediments using the alkylammonium method. Clay Minerals, 20, 291-300.

Sangüesa, F.J. (1998) La diagénesis en el Bloque Alavés de la Cuenca Vasco-Cantábrica. Distribución, modelización y aplicaciones. Ph.D. thesis, 160 pp. University of the Basque Country, Bilbao, Spain.

Sangüesa, F.J., Aróstegui, J., and Suárez-Ruiz, I. (2000) Distribution and origin of clay minerals in the Lower Cretaceous of the Alava Block (Basque-Cantabrian Basin, Spain). Clay Minerals, 35, 393-410.

Sato, T., Murakami, T., and Watanabe, T. (1996) Change in layer charge of smectites and smectite layers in illite/smectite during diagenetic alteration. Clays and Clay Minerals, 44, 460-469.

Schumann, D., Hesse, R., Sears, S.K., and Vali, H. (2014) Expansion behavior of

octadecylammonium-exchanged low-to high-charge reference smectite-group minerals as revealed by high-resolution transmission electron microscopy on ultrathin sections. Clays and Clay Minerals, 62, 336-353.

Sears, S.K., Hesse, R., and Vali, H. (1998) Significance of n-alkylammonium exchange in the study of 2:1 clay mineral diagenesis, Mackenzie Delta Beaufort Sea region, Arctic Canada. Canadian Mineralogist, 36, 1485-1506.

Shata, S., Hesse, R., Martin, R.F., and Vali, H. (2003) Expandability of anchizonal illite and chlorite: Significance for crystallinity development in the transition from diagenesis to metamorphism. American Mineralogist, 88, 748-762.

Srodon, J., and Eberl, D. (1984) Illite. In S.W. Bailey, Ed. Micas. Reviews in Mineralogy., 13. Min. Soc. Amer.

Vali, H., and Hesse, R. (1990) Alkylammonium ion treatment of clay-minerals in ultrathin section - a new method for HRTEM examination of expandable layers. American Mineralogist, 75, 1443-1446.

Vali, H., Hesse, R., and Martin, R.F. (1994) A TEM-based definition of 2-1 layer silicates and their interstratified constituents. American Mineralogist, 79, 644-653.

Vali, H., and Köster, H.M. (1986) Expanding behaviour, structural disorder, regular and ramdom irregular interestratification of 2:1 layer-silicates studied by high-resolution images of transmission electron microscopy. Clay Minerals, 21, 827-859.

Wolters, F., Lagaly, G., Kahr, G., Nueesch, R., and Emmerich, K. (2009) A comprehensive characterization of dioctahedral smectites. Clays and Clay Minerals, 57, 115-133.

761 **Figure Captions**

762 **Figure 1.** Evolution with depth of the type of order and %S layers of the I/S in the two study
763 sections: CS and KG. Blank symbols: major R0 type. Solid symbols: major R1 type and
764 absence of R0.

765

766 **Figure 2.** XRD diagrams of two representative samples intercalated with the complete series
767 of *n*-alkylammonium. Left: sample 1CS6, an example of the R0 stadium. Right: sample
768 3CS3, representative of the R1 stadium.

769

770 **Figure 3.** Decomposition of 1CS6 profiles, corresponding to samples treated with
771 alkylammonium with a chain length of n_c:8, n_c:9, and n_c:11. The interpretation of all the
772 diagrams shown in Fig. 2 (left) was supported by similar decompositions.

773

774 **Figure 4.** Decomposition of 3CS3 profiles, corresponding to samples treated with
775 alkylammonium with a chain length of n_c:7 and n_c:10. The interpretation of all the diagrams
776 shown in Fig. 2 (right) was supported by similar decompositions.

777

778 **Figure 5.** Measured d_{001} spacing for the different chain lengths of alkylammonium for
779 samples 1CS6, 2KG6, 3CS3, and 3CS6. The existence of two smectites with different layer
780 charges is deduced for samples 1CS6 and 2KG6 based on monolayer-bilayer transitions with
781 different chain lengths (see Fig. 3).

782

783 **Figure 6.** Low-magnification image showing the typical texture of samples cut with the
784 diamond knife and treated with *n*-alkylammonium.
785
786 **Figure 7.** Representative lattice-fringe image of sample 1CS6 treated with n_c:8-
787 alkylammonium. Basal spacing in the range of 13-14 Å is characteristic of a monolayer
788 configuration.
789
790 **Figure 8.** Typical lattice-fringe image of sample 2KG6 treated with n_c:8- alkylammonium.
791 R0 I/S has basal spacing of around 13.5 Å, characteristic of a monolayer configuration, or
792 18 Å, characteristic of a bilayer configuration. The lower part of the image also shows I1
793 I/S, with a d_{001} spacing of 27 Å, which is the sum of one illite and one smectite with bilayer
794 configuration units.
795
796 **Figure 9.** Characteristic lattice-fringe image of sample 2KG6 treated with n_c:14-
797 alkylammonium. Smectite has basal spacing of around 18 Å, characteristic of a bilayer
798 configuration, or 22 Å, characteristic of a pseudotrilayer configuration. The lower part of the
799 image also shows I1 I/S, with a d_{001} spacing of 28 Å, which is the sum of one illite and one
800 smectite with bilayer configuration units. A part of this I1 I/S laterally grades to R0 I/S. One
801 extra smectitic layer remains in the 28 Å I/S packet.
802
803 **Figure 10.** Representative lattice-fringe image of sample 3CS3 treated with n_c:8-
804 alkylammonium. R1 I/S shows basal spacing that represents the sum of one smectitic layer
805 with a monolayer configuration (14 Å) plus one, two, or three unexpanded 10 Å illite layers.
806

807 **Figure 11.** a) Lattice-fringe image of sample 3CS3 treated with n_c:14- alkylammonium,
808 showing domains with I≥3 I/S, formed by various layers of unexpanded illite (10 Å) and one
809 smectitic layer with bilayer or pseudotrilayer configurations (18 or 21 Å). b) Representative
810 lattice-fringe image of sample 3CS6 treated with n_c:14- alkylammonium. R1 I/S shows basal
811 spacing that represents the sum of one smectite layer with a bilayer configuration (17-18 Å)
812 plus one 10 Å illite layer.
813
814 **Figure 12.** Comparison between the type of interlayer alkylammonium configuration
815 determined by XRD and those deduced from d_{001} values measured on lattice-fringe images
816 obtained on TEM for samples treated with n_c:8 and n_c:14 alkylammonium. The sketches for
817 R1 and R>3 (I1 and I>3) represent only the corresponding smectitic layer of the I/S.
818
819 **Figure 13.** Comparison between layer charge obtained by XRD on alkylammonium-treated
820 samples and the average values from formulae obtained by AEM. R1 I/S include only the
821 charge corresponding to the expandable layers.
822
823 **Table 1.** Layer charge of samples of the R0 and R1 stages for the <2 μm and <0.5 μm
824 fraction specimens and corresponding versions after the Hofmann-Klemen treatment with Li
825 (Greene-Kelly 1952). The values were obtained through the procedure illustrated in Figures
826 2, 3, 4, and 5 using the software XCharge (Hofmann et al. 2002), which follows the
827 procedure by Lagaly (1994).
828
829 **Table 2.** Chemical compositions of smectite or R0 I/S.
830

831 **Table 3.** Chemical compositions of R1 I/S.

832

		< 2 μm		< 2 μm + Li		< 0.5 μm		< 0.5 μm + Li	
R0 Samples	% Sm	ξ Sm1	ξ Sm2	ξ Sm1	ξ Sm2	ξ Sm1	ξ Sm2	ξ Sm1	ξ Sm2
1CS6	90%	0.33	0.37	0.27	0.34	0.32	0.37	0.28	0.32
1KG5	90%	0.32	0.37	0.28	-	0.32	0.34	0.27	-
1CS9	70%	0.38	0.41	0.32	0.41	0.37	0.41	0.27	0.41
2KG3	70%	0.38	0.41	0.32	0.41	0.37	0.39	0.29	0.34
2KG6	65%	0.39	0.41	0.32	0.41	0.37	0.39	0.29	0.34
R1 Samples		ξ Sm		ξ Sm		ξ Sm		ξ Sm	
3CS3	35	0.36		0.36		0.35		0.33	
3KG5	35	0.33		0.29		0.32		0.31	
3CS6	30	0.38		0.34		0.37		0.36	

Note: ξ character refer to the layer charge / $(Si, Al)_4 O_{10}$

Sample	Si	^{IV}Al	^{VI}Al	Fe[a]	Mg	**Σoct.**	K	Na	Ca	**Σint.**
Smectite (R0 stadium)										
1CS6-1-1	3.55	0.45	1.64	0.21	0.24	**2.1**	0.2	0.1	0.05	**0.4**
1CS6-15-15	3.61	0.39	1.58	0.22	0.28	**2.08**	0.24	0.09	0.05	**0.43**
1CS6-1b	3.57	0.43	1.7	0.17	0.21	**2.09**	0.16	0.16	0.03	**0.38**
1CS6-3b	3.59	0.41	1.86	0.07	0.12	**2.05**	0.12	0.17	0.05	**0.38**
1CS6-4b	3.76	0.24	1.54	0.23	0.24	**2.01**	0.21	0.1	0.07	**0.45**
1CS6-5b	3.9	0.1	1.57	0.19	0.22	**1.99**	0.21	0.05	0.05	**0.36**
1CS6-6b	3.85	0.15	1.73	0.1	0.17	**2.01**	0.23	0	0.03	**0.3**
1CS6-7b	3.76	0.24	1.77	0.05	0.17	**2**	0.19	0.09	0.07	**0.42**
1CS6-9b	3.87	0.13	1.66	0.14	0.17	**1.97**	0.21	0.07	0.05	**0.38**
1CS6-10b	3.68	0.32	1.48	0.35	0.22	**2.05**	0.23	0.07	0.05	**0.4**
1CS6-16-16	3.76	0.24	1.79	0.1	0.15	**2.04**	0.15	0.05	0.03	**0.27**
1CS9-1-5	3.74	0.26	1.65	0.14	0.26	**2.05**	0.12	0.12	0.07	**0.38**
1CS9-8-12	3.86	0.14	1.68	0.12	0.22	**2.02**	0.14	0.09	0.03	**0.3**
1CS9-10-14	3.72	0.28	1.67	0.1	0.26	**2.03**	0.16	0.12	0.09	**0.45**
1CS9-11-15	3.74	0.26	1.73	0.09	0.19	**2**	0.2	0.14	0.05	**0.44**
1CS9-13-17	3.74	0.26	1.7	0.12	0.21	**2.03**	0.2	0.05	0.07	**0.39**
1KG5-7-10	3.77	0.23	1.61	0.17	0.3	**2.08**	0.17	0.05	0.03	**0.3**
1KG5-9-12	3.75	0.25	1.64	0.16	0.26	**2.06**	0.2	0.07	0.03	**0.33**
1KG5-10-13	3.58	0.42	1.54	0.25	0.32	**2.1**	0.3	0.07	0.04	**0.44**
1KG5-12-1	3.64	0.36	1.65	0.17	0.24	**2.06**	0.31	0.07	0.02	**0.41**
1KG5-11b	3.77	0.23	1.59	0.19	0.26	**2.04**	0.12	0.1	0.07	**0.36**
1KG5-12b	3.84	0.16	1.49	0.28	0.26	**2.02**	0.14	0.12	0.05	**0.36**
1KG5-13b	3.83	0.17	1.4	0.35	0.26	**2.01**	0.26	0.05	0.05	**0.42**
1KG5-14b	3.74	0.26	1.56	0.24	0.28	**2.08**	0.17	0.05	0.03	**0.29**
1KG5-16b	3.89	0.11	1.49	0.21	0.29	**1.99**	0.16	0.05	0.1	**0.42**
1KG5-17b	3.72	0.28	1.44	0.31	0.33	**2.08**	0.21	0.09	0.03	**0.37**
1KG5-18b	3.89	0.11	1.51	0.22	0.29	**2.02**	0.19	0.03	0.05	**0.33**
2KG3-1-6	3.61	0.39	1.68	0.12	0.24	**2.04**	0.24	0.19	0.03	**0.5**
2KG3-4-9	3.58	0.42	1.85	0.09	0.12	**2.06**	0.09	0.14	0.07	**0.36**
2KG3-6-11	3.83	0.17	1.54	0.21	0.26	**2.01**	0.17	0.05	0.09	**0.4**
2KG3-9-14	3.69	0.31	1.51	0.17	0.38	**2.07**	0.14	0.21	0.07	**0.49**
2KG3-11-16	3.86	0.14	1.58	0.21	0.24	**2.03**	0.09	0.07	0.07	**0.29**
2KG3-12-17	3.75	0.25	1.58	0.17	0.26	**2.01**	0.28	0.1	0.05	**0.49**
2KG3-13-18	3.78	0.22	1.63	0.15	0.22	**2.01**	0.2	0.15	0.03	**0.42**
2KG3-15-20	3.92	0.08	1.52	0.21	0.29	**2.02**	0.07	0.08	0.09	**0.32**
2KG6-1-1	3.58	0.42	1.86	0.05	0.16	**2.06**	0.19	0.09	0.05	**0.38**
2KG6-2-2	3.65	0.35	1.57	0.21	0.26	**2.03**	0.21	0.05	0.12	**0.5**
2KG6-3-3	3.7	0.3	1.8	0.05	0.15	**2**	0.09	0.25	0.05	**0.44**
2KG6-4-4	3.47	0.53	1.85	0.1	0.12	**2.08**	0.23	0.07	0.05	**0.41**
2KG6-7-7	3.65	0.35	1.35	0.43	0.28	**2.06**	0.21	0.09	0.07	**0.44**
2KG6-11-11	3.57	0.43	1.73	0.1	0.24	**2.07**	0.27	0.07	0.05	**0.45**
2KG6-12-12	3.7	0.3	1.7	0.1	0.24	**2.05**	0.14	0.05	0.1	**0.4**
2KG6-15-3	3.74	0.26	1.81	0.05	0.15	**2.01**	0.22	0.05	0.05	**0.38**

Notes: Composition normalized to $O_{10}OH_2$ Σoct.= Sum of octahedral cations. Σint.= Sum of interlayer charge.

[a] All Fe considered as Fe^{3+}

Sample	Si	^{IV}Al	^{VI}Al	Fe[a]	Mg	**Σoct**	K	Na	Ca	**Σint.**
R1 I/S (R0 stadium)										
1CS6-3-3	3.45	0.55	1.59	0.23	0.21	**2.03**	0.45	0.12	0.05	**0.68**
1CS6-4-4	3.45	0.55	1.68	0.14	0.21	**2.03**	0.28	0.32	0.03	**0.67**
1CS6-5-5	3.33	0.67	1.33	0.46	0.32	**2.11**	0.41	0.14	0.05	**0.66**
1CS6-6-6	3.57	0.43	1.59	0.21	0.19	**1.99**	0.49	0.11	0.03	**0.66**
1CS6-9-9	3.5	0.5	1.52	0.25	0.3	**2.07**	0.4	0.05	0.07	**0.6**
1CS6-11-11	3.48	0.52	1.68	0.19	0.21	**2.08**	0.33	0.09	0.03	**0.49**
1CS6-14-14	3.52	0.48	1.53	0.28	0.26	**2.07**	0.3	0.12	0.05	**0.53**
1CS6-12-12	3.54	0.46	1.37	0.35	0.32	**2.04**	0.39	0.12	0.07	**0.65**
1CS9-2-6	3.61	0.39	1.56	0.14	0.31	**2.02**	0.26	0.25	0.07	**0.65**
1CS9-3-7	3.55	0.45	1.49	0.23	0.35	**2.07**	0.3	0.19	0.05	**0.6**
1CS9-4-8	3.64	0.36	1.58	0.12	0.3	**2**	0.26	0.27	0.07	**0.67**
1CS9-14-1	3.59	0.41	1.46	0.25	0.32	**2.02**	0.42	0.14	0.05	**0.67**
1KG5-13-2	3.58	0.42	1.55	0.21	0.28	**2.04**	0.3	0.12	0.07	**0.56**
1KG5-14-3	3.48	0.52	1.56	0.23	0.3	**2.08**	0.44	0.05	0.04	**0.56**
2KG3-3-8	3.45	0.55	1.63	0.19	0.25	**2.07**	0.33	0.12	0.07	**0.6**
2KG3-7-12	3.43	0.57	1.73	0.16	0.21	**2.1**	0.14	0.18	0.09	**0.49**
2KG3-8-13	3.45	0.55	1.6	0.17	0.24	**2.02**	0.38	0.18	0.09	**0.74**
2KG3-10-15	3.47	0.53	1.48	0.3	0.26	**2.05**	0.28	0.19	0.09	**0.65**
2KG3-16-21	3.4	0.6	1.74	0.1	0.16	**2**	0.38	0.26	0.05	**0.75**
2KG6-5-5	3.57	0.43	1.78	0.09	0.14	**2**	0.26	0.24	0.03	**0.56**
2KG6-6-6	3.45	0.55	1.15	0.61	0.32	**2.07**	0.3	0.18	0.09	**0.65**
2KG6-9-9	3.51	0.49	1.77	0.09	0.16	**2.01**	0.51	0.03	0.03	**0.62**
2KG6-10-10	3.64	0.36	1.64	0.12	0.24	**2**	0.38	0.12	0.05	**0.61**
R1 I/S (R1 stadium)										
3CS3-4-19	3.39	0.61	1.76	0.09	0.19	**2.04**	0.44	0.12	0.05	**0.67**
3CS3-8-23	3.52	0.48	1.79	0.07	0.14	**1.99**	0.47	0.11	0.03	**0.64**
3CS3-9-24	3.45	0.55	1.8	0.05	0.21	**2.07**	0.37	0.09	0.05	**0.56**
3CS3-12-27	3.4	0.6	1.76	0.05	0.25	**2.06**	0.43	0.14	0.05	**0.67**
3CS6-5-8	3.5	0.5	1.83	0.07	0.17	**2.07**	0.17	0.16	0.07	**0.46**
3CS6-4-4	3.32	0.68	1.95	0.02	0.05	**2.02**	0.5	0.14	0.02	**0.67**
3CS6-13-13	3.5	0.5	1.9	0.03	0.07	**2.01**	0.29	0.18	0.03	**0.54**
3KG5-2-21	3.52	0.48	1.59	0.16	0.31	**2.06**	0.4	0.12	0.05	**0.63**
3KG5-4-23	3.53	0.47	1.68	0.09	0.24	**2.01**	0.48	0.09	0.05	**0.67**
3KG5-11-30	3.6	0.4	1.57	0.21	0.26	**2.04**	0.27	0.18	0.05	**0.55**
3KG5-12-31	3.48	0.52	1.69	0.14	0.17	**2**	0.5	0.13	0.03	**0.7**
3KG5-15-34	3.55	0.45	1.76	0.07	0.17	**2**	0.23	0.18	0.1	**0.62**
3KG5-17-36	3.46	0.54	1.66	0.17	0.19	**2.03**	0.46	0.09	0.05	**0.65**
3KG5-37b	3.41	0.59	1.8	0.09	0.17	**2.06**	0.48	0.07	0.02	**0.58**
3KG5-1	3.46	0.54	1.59	0.17	0.26	**2.03**	0.52	0.09	0.05	**0.71**
3KG5-6	3.44	0.56	1.61	0.21	0.26	**2.08**	0.49	0.02	0.04	**0.58**
3KG5-7	3.33	0.67	1.75	0.12	0.21	**2.09**	0.48	0.11	0.02	**0.62**
3KG5-10	3.24	0.76	1.77	0.16	0.17	**2.1**	0.42	0.11	0.05	**0.63**
3KG5-11	3.45	0.55	1.47	0.31	0.31	**2.1**	0.32	0.09	0.09	**0.58**
3KG5-12	3.36	0.64	1.79	0.12	0.19	**2.1**	0.46	0.03	0.02	**0.53**

Notes: Composition normalized to O_{10} OH_2. Σoct.= Sum of octahedral cations. Σ int.= Sum of interlayer charge.

[a] All Fe considered as Fe^{3+}

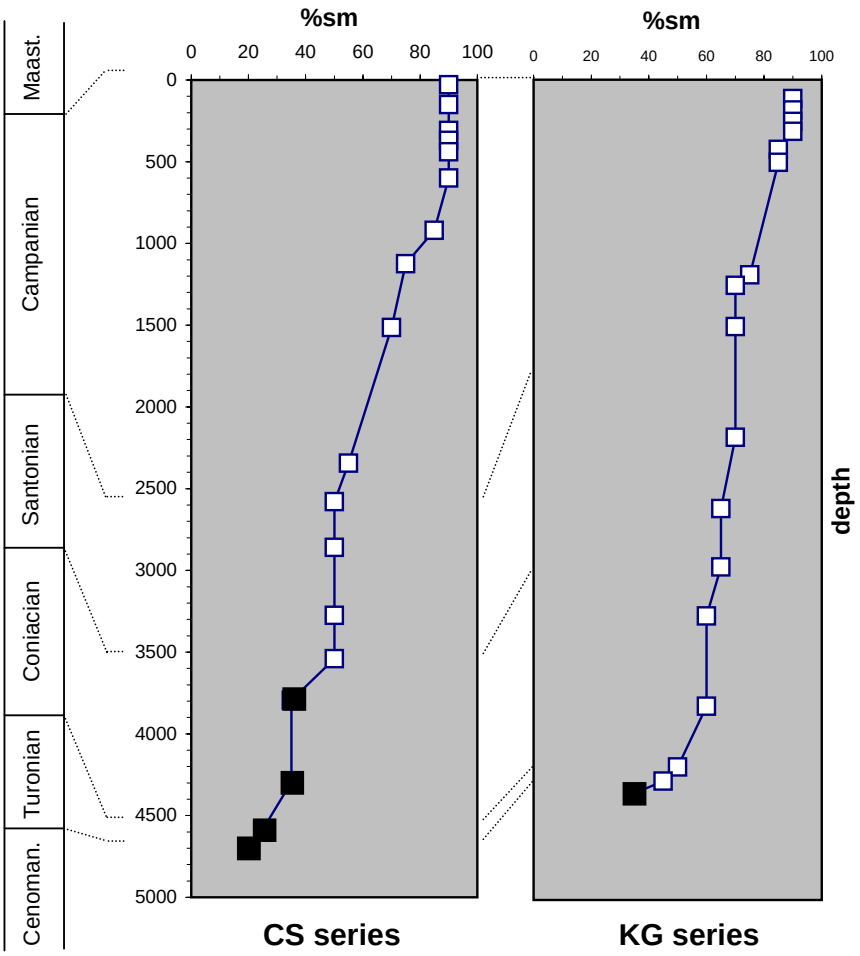
Maast.
Campanian
Santonian
Coniacian
Turonian
Cenoman.
%sm
0
20
40
60
80
100
0
500
1000
1500
2000
2500
3000
3500
4000
4500
5000
CS series
%sm
0
20
40
60
80
100
KG series
depth

FIGURE 1

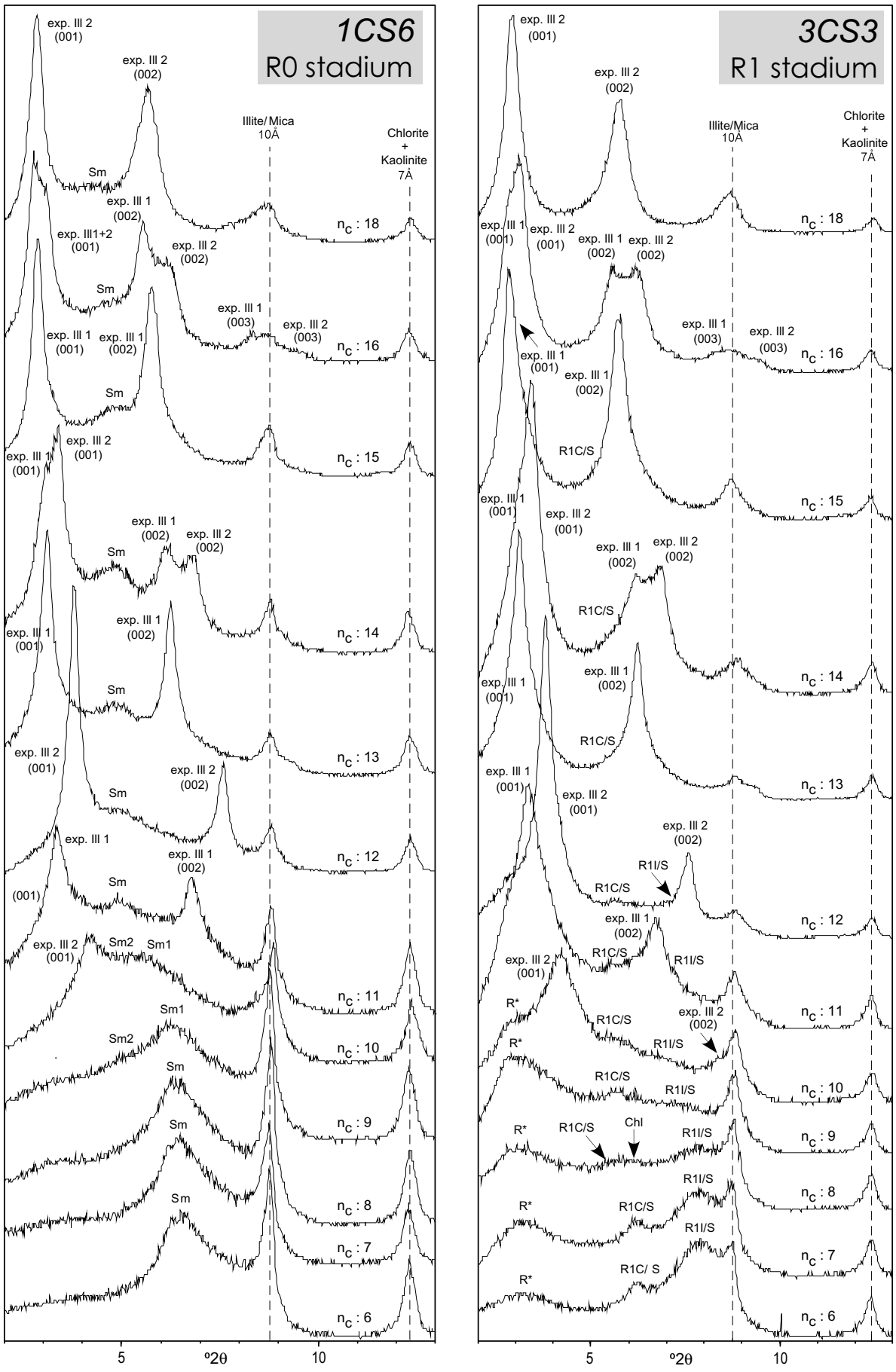
1CS6
R0 stadium
3CS3
R1 stadium
Illite/Mica 10Å
Chlorite + Kaolinite 7Å
exp. III 2 (001)
exp. III 2 (002)
exp. III 1 (002)
exp. III1+2 (001)
exp. III 1 (003)
exp. III 2 (003)
exp. III 1 (001)
Sm
Sm1
Sm2
R1C/S
R1I/S
R*
Chl
nc : 18
nc : 16
nc : 15
nc : 14
nc : 13
nc : 12
nc : 11
nc : 10
nc : 9
nc : 8
nc : 7
nc : 6
5
º2θ
10

FIGURE 2

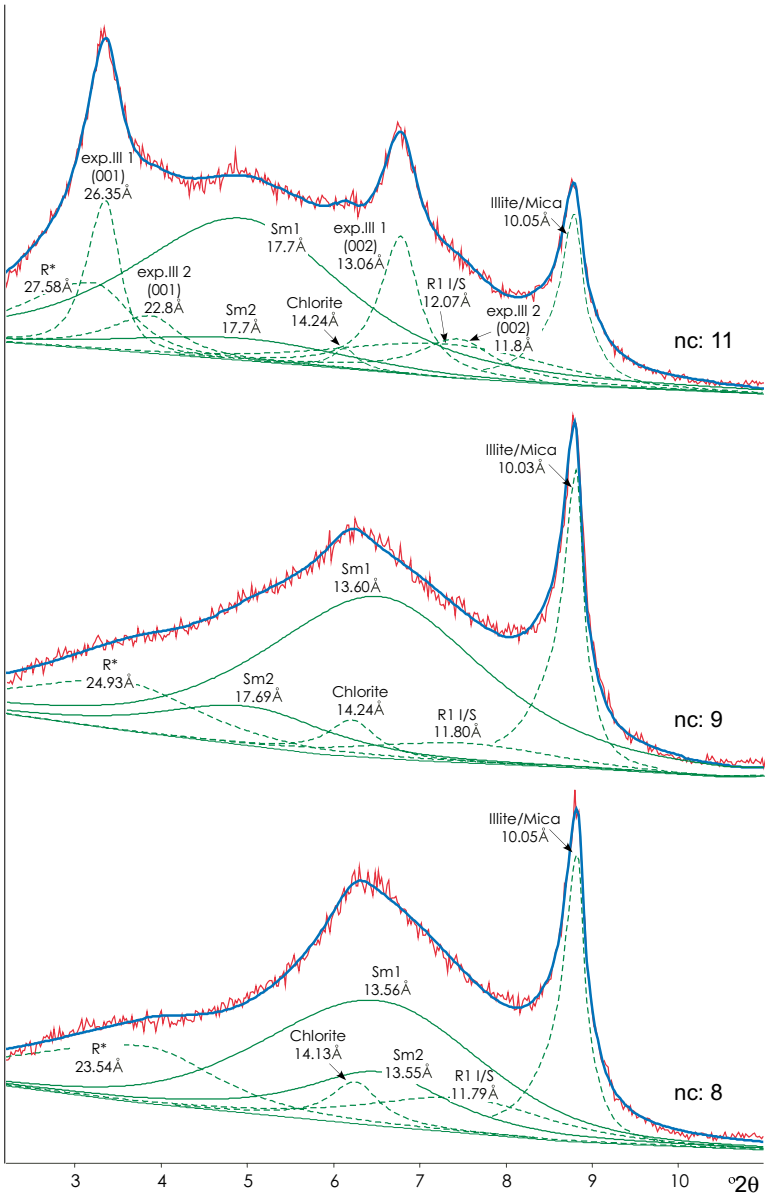
exp.Ill 1
(001)
26.35Å
R*
27.58Å
exp.Ill 2
(001)
22.8Å
Sm1
17.7Å
Sm2
17.7Å
Chlorite
14.24Å
exp.Ill 1
(002)
13.06Å
R1 I/S
12.07Å
exp.Ill 2
(002)
11.8Å
Illite/Mica
10.05Å
nc: 11
Illite/Mica
10.03Å
Sm1
13.60Å
R*
24.93Å
Sm2
17.69Å
Chlorite
14.24Å
R1 I/S
11.80Å
nc: 9
Illite/Mica
10.05Å
Sm1
13.56Å
R*
23.54Å
Chlorite
14.13Å
Sm2
13.55Å
R1 I/S
11.79Å
nc: 8
3
4
5
6
7
8
9
10
°2θ

FIGURE 3

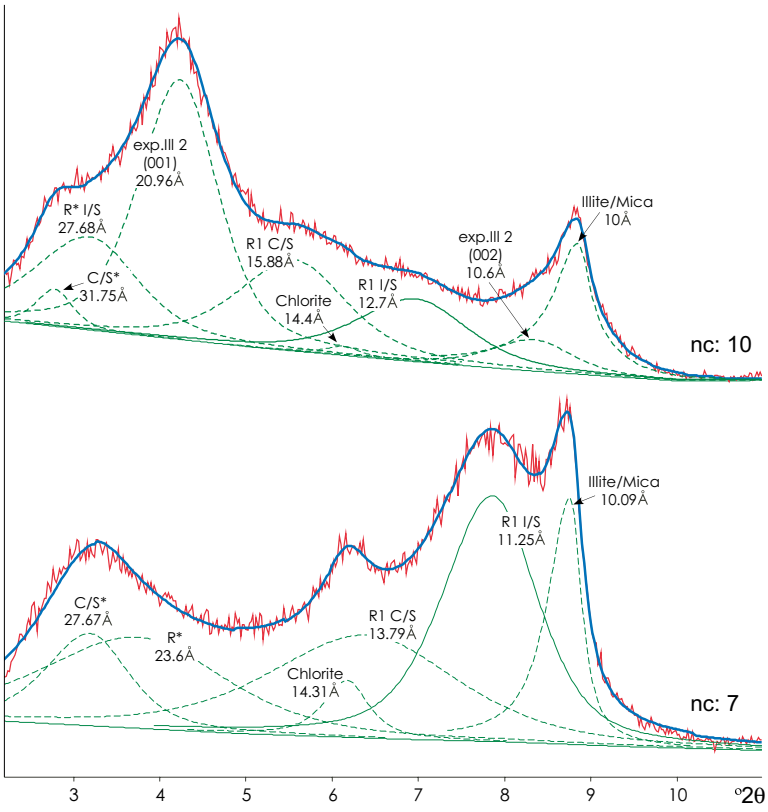
exp.Ill 2
(001)
20.96Å
R* I/S
27.68Å
C/S*
31.75Å
R1 C/S
15.88Å
Chlorite
14.4Å
R1 I/S
12.7Å
exp.Ill 2
(002)
10.6Å
Illite/Mica
10Å
nc: 10
C/S*
27.67Å
R*
23.6Å
Chlorite
14.31Å
R1 C/S
13.79Å
R1 I/S
11.25Å
Illite/Mica
10.09Å
nc: 7
3
4
5
6
7
8
9
10
°2θ

FIGURE 4

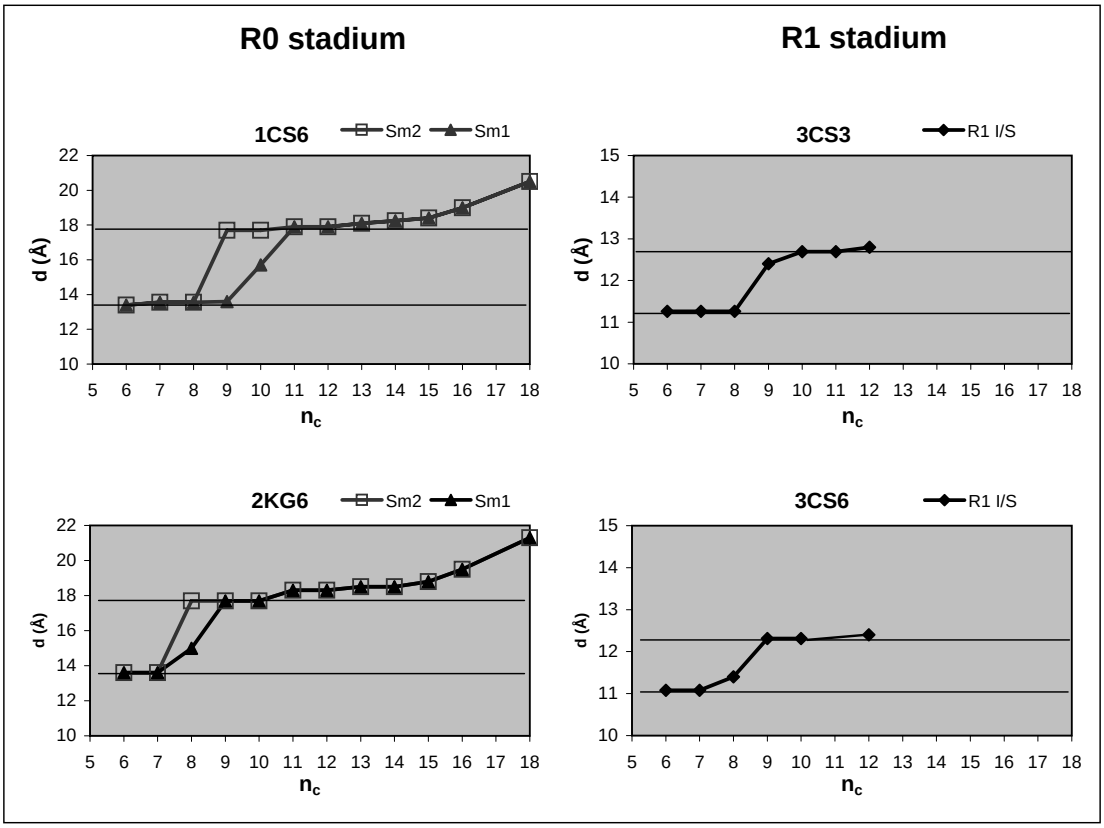
R0 stadium
R1 stadium
1CS6
Sm2
Sm1
3CS3
R1 I/S
2KG6
Sm2
Sm1
3CS6
R1 I/S
d (Å)
n_c

FIGURE 5

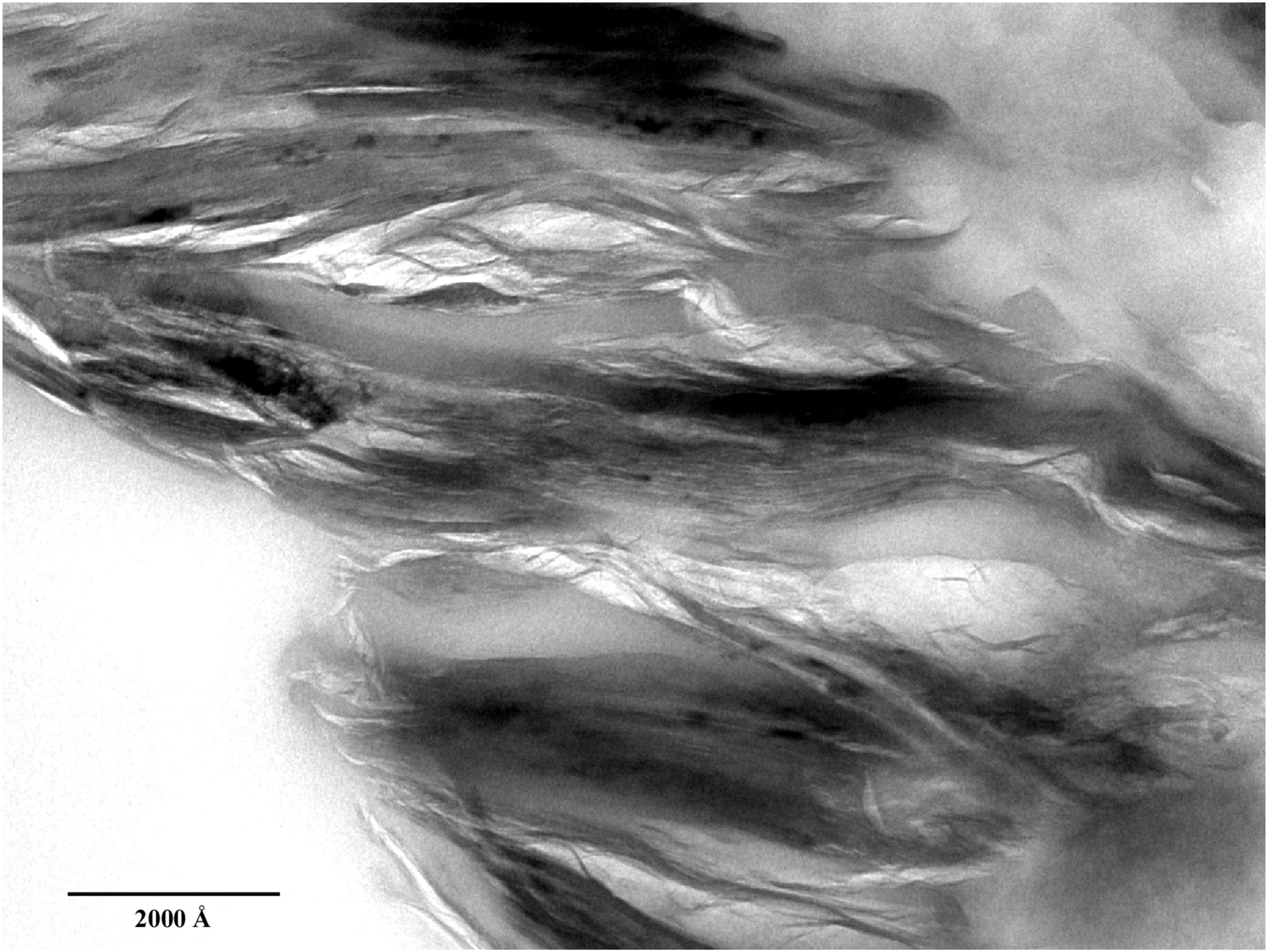
2000 Å

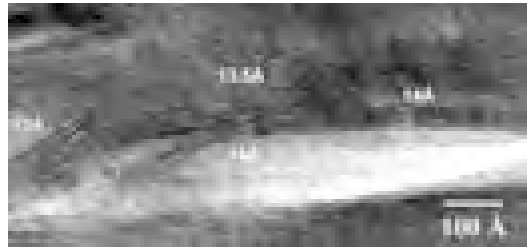
100 Å

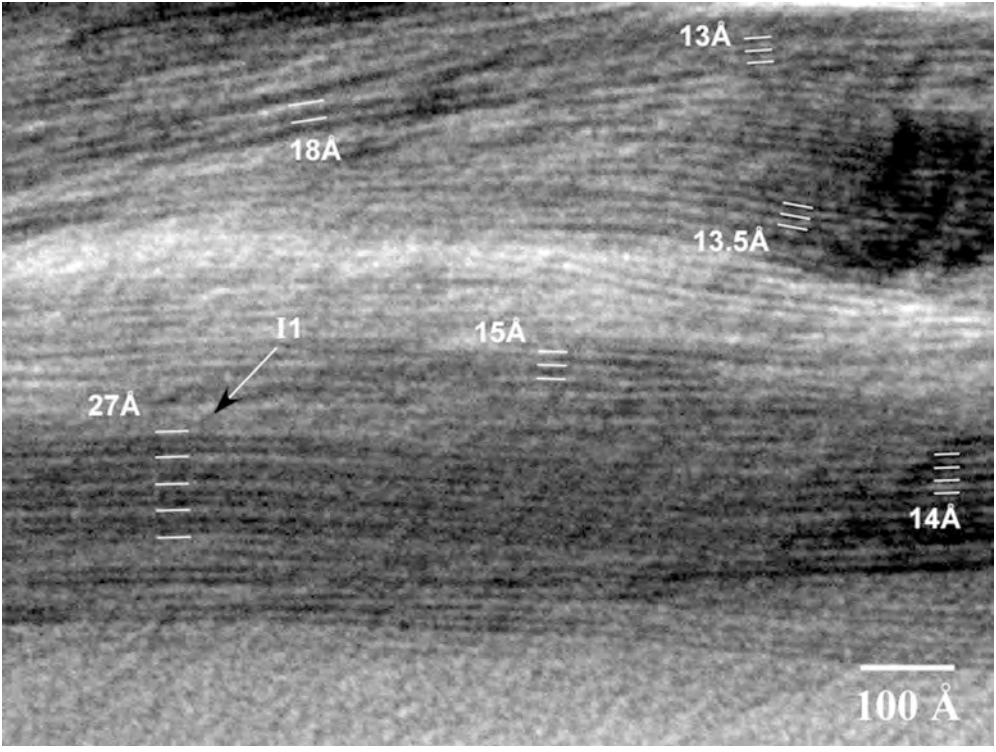
13Å
18Å
13.5Å
I1
15Å
27Å
14Å
100 Å

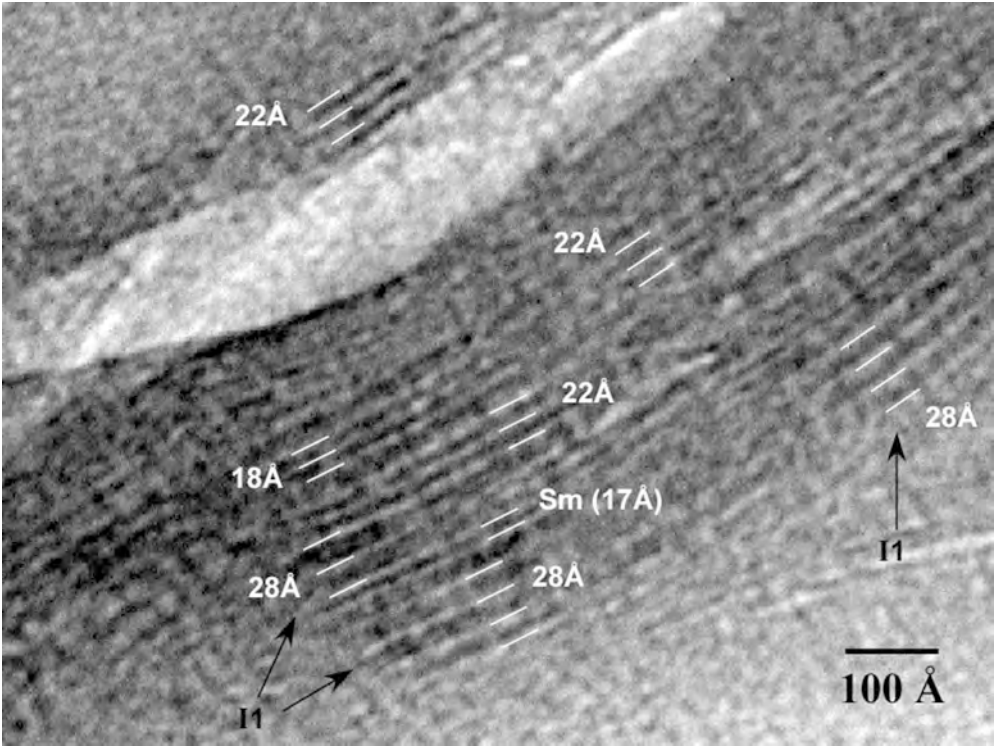
22Å
22Å
22Å
28Å
18Å
Sm (17Å)
28Å
28Å
I1
I1
100 Å

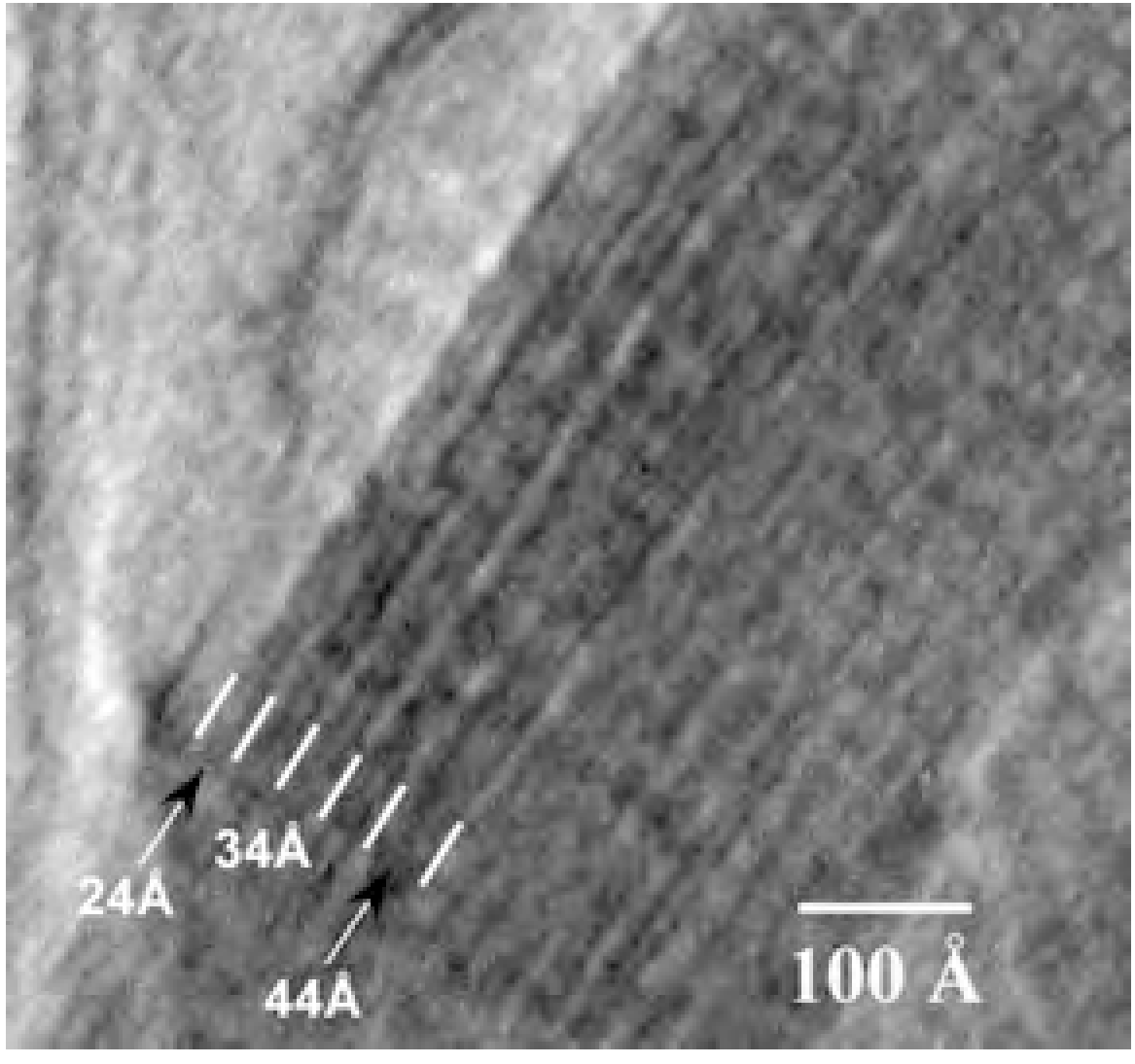
24A
34A
44A
100 Å

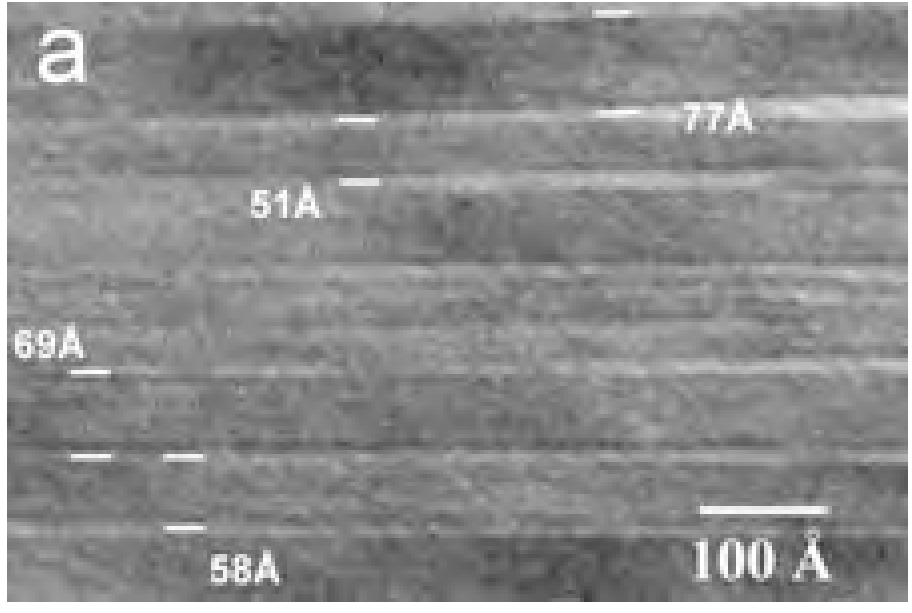
a
77Å
51Å
69Å
58Å
100 Å


b

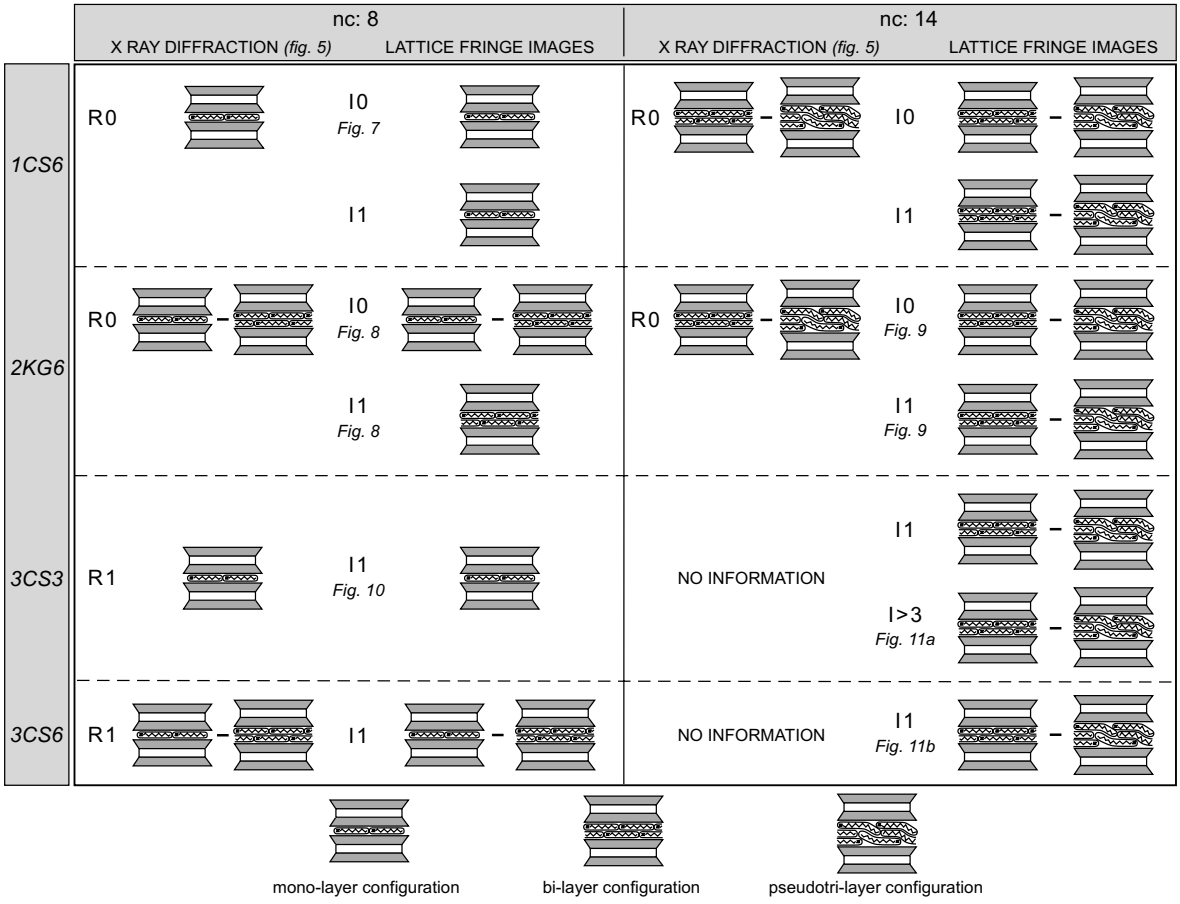
nc: 8
X RAY DIFFRACTION (fig. 5)
LATTICE FRINGE IMAGES
nc: 14
X RAY DIFFRACTION (fig. 5)
LATTICE FRINGE IMAGES
1CS6
2KG6
3CS3
3CS6
R0
I0
Fig. 7
I1
R0
I0
I1
R0
I0
Fig. 8
I1
Fig. 8
R0
I0
Fig. 9
I1
Fig. 9
R1
I1
Fig. 10
NO INFORMATION
I1
I>3
Fig. 11a
R1
I1
NO INFORMATION
I1
Fig. 11b
mono-layer configuration
bi-layer configuration
pseudotri-layer configuration

Fig. 12

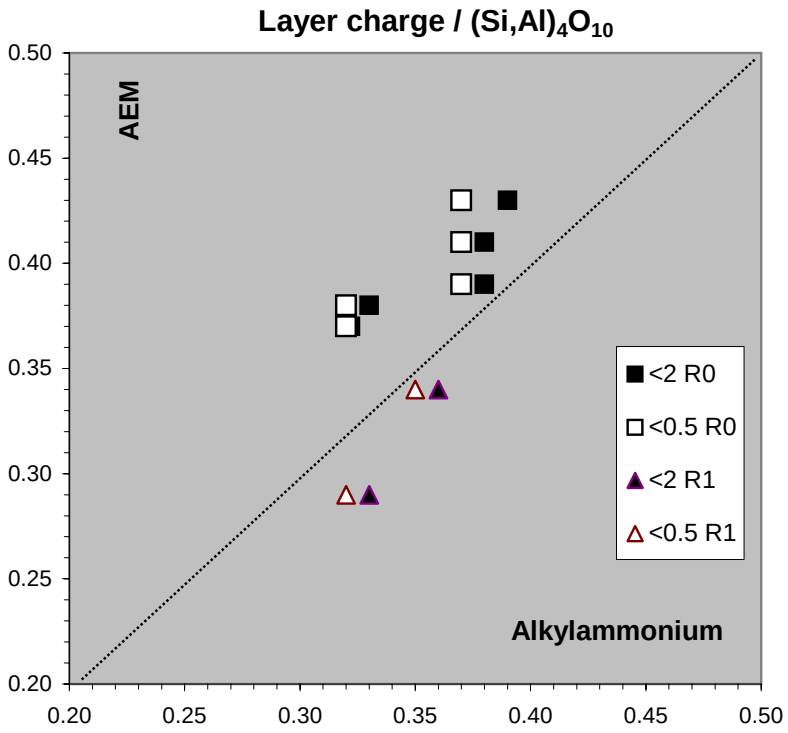
Layer charge / (Si,Al)4O10
0.50
0.45
0.40
0.35
0.30
0.25
0.20
0.20
0.25
0.30
0.35
0.40
0.45
0.50
AEM
Alkylammonium
<2 R0
<0.5 R0
<2 R1
<0.5 R1

FIGURE 13